

Kinetic Theory of Cosmological Magnetogenesis at Second Order: A New Density-Gradient Source and Comparison with the Harrison Mechanism

Bob Osano^{1,2}

¹Cosmology and Gravity Group, Department of Mathematics and Applied Mathematics,
University of Cape Town, Rondebosch 7701, South Africa

²Centre for Higher Education Development, University of Cape Town, Rondebosch 7701, South
Africa

Correspondence: bob.osano@uct.ac.za

June 16, 2026

Abstract

We derive and compare three mechanisms of cosmological magnetogenesis: the Thomson-scattering velocity-difference mechanism of Takahashi et al. (2005), a new density-gradient source identified here for the first time, and the Harrison bulk-flow mechanism of Cembranos et al. (2020). Starting from the coupled Maxwell–Boltzmann equations, the complete kinetic theory chain is derived in a single document—from the BBGKY hierarchy and Thomson collision term, through the generalised Ohm’s law, to the second-order magnetic induction equation. The Ohm’s law correction terms are each bounded by $m_e/m_p \approx 5.4 \times 10^{-4}$, confirming the standard single-fluid approximation to better than 0.1%. At second order in cosmological perturbations, products of first-order scalar source vorticity; we identify a coupling between the photon density contrast $\delta_\gamma \equiv \delta\rho_\gamma^{(1)}/\bar{\rho}_\gamma$ and the electron–photon velocity difference $(u_e - u_\gamma)^{(1)}$ that was implicitly present in previous treatments but never isolated. Numerical evaluation with CAMB v1.6.6 at $z = 1100$ shows that this term contributes at $\approx 0.97 \times B_{\text{Tak}}$, giving a scattering-mechanism total $\approx 1.4 \times$ the Takahashi result. The Harrison mechanism at the Planck bulk-flow limit ($\beta < 8.5 \times 10^{-4}$) yields $B \approx 5.7 \times 10^{-24}$ G at 1 Mpc today and dominates for $\beta \gtrsim 2 \times 10^{-3}$, mildly above the Planck limit. All seed fields exceed the galactic dynamo threshold by many orders of magnitude.

Keywords: cosmological magnetogenesis; kinetic theory; Boltzmann equation; Thomson scattering; Harrison mechanism; second-order perturbations; galactic dynamo.

Contents

1	Introduction	4
2	Cosmological Framework	6
3	Kinetic Theory	7
3.1	One-particle distribution function and the BBGKY hierarchy	7
3.2	Equilibrium distributions and the H-theorem	8
3.3	Relativistic kinetic theory in curved spacetime	9
3.4	Boltzmann equation: collision term and moment hierarchy	11
4	The Scattering Mechanism: Collision Terms and Euler Equations	13
4.1	Setup: projection formalism and Euler equations with collisions	13
4.2	Why Coulomb terms cause decay, not growth	15
4.3	Thomson scattering: cross-section and matrix element	16
4.4	Evaluation of the Thomson collision term	17
4.5	Euler equations for the charged species	20
5	The Harrison Bulk-Flow Mechanism	20
5.1	Differential spin-down	20
5.2	Notation and plasma setup	21
5.3	Thomson coupling with bulk flows	22
5.4	Complete evolution equation for the magnetic field	22
5.5	Vorticity evolution	23
5.6	Order-of-magnitude estimate	24
6	Generalised Ohm’s Law	24
6.1	Derivation from the charged-species Euler equations	24
6.2	Estimate of correction terms	25
7	Perturbed FLRW Metric	25
7.1	Why vector and tensor modes first appear at second order	25
7.2	Metric decomposition	26

8	Second-Order Magnetic Field Evolution	26
8.1	From the Bianchi identity to the induction equation	26
8.2	Perturbative expansion and the linear vorticity constraint	27
8.3	The second-order source term	27
8.4	The second-order vorticity and the proportionality constant	27
9	Fourier-Space Representation and Power Spectrum	28
9.1	Scalar harmonic decomposition	28
9.2	Second-order magnetic field in Fourier space	29
9.3	Power spectrum bound	29
9.4	Numerical results: magnetic power spectrum	30
10	Discussion	30
10.1	Scattering mechanism: field strength and decay	30
10.2	Harrison mechanism: field strength	34
10.3	Comparison and the galactic dynamo threshold	34
11	Conclusions	34
A	Anisotropic Stress Contraction	37
B	Four-Velocity	37
C	Mass-Shell Condition	38
D	Cosmological Parameters	38

1 Introduction

The presence of magnetic fields across a wide range of astrophysical and cosmological scales is well established and substantiated by diverse observational studies. Recent research indicates that such fields on cosmological scales may be more pervasive than previously thought [1]. Detection methods include the Faraday rotation effect in linearly polarised sources [2–4], the deflection of cosmic rays [5, 6], and temperature and polarisation anisotropies of the CMB [7–16]. Residual effects on elemental abundances during Big Bang Nucleosynthesis [17] and electromagnetic cascades from blazars [1] provide further, indirect constraints.

Any meaningful study of cosmological magnetic fields must address two challenges: (i) the *generation* of seed fields, and (ii) their *sustenance* against dilution in an expanding universe. The generation problem primarily concerns producing vorticity sufficient to exceed the minimum threshold required by natural amplifiers such as the galactic dynamo. This threshold and the origin of the seed field have remained persistent open questions [18–23].

Candidate seed-field sources include the Biermann battery effect [17, 24], arising from pressure gradients in ionisation fronts during reionisation ($z \gtrsim 5$); Hall’s effect [25]; and the Harrison mechanism [26], in which differential rotation between the proton and radiation fluids generates vorticity. Once produced, seed fields may be amplified by inverse cascading, galactic, or mean-field dynamos [27–30]

Takahashi [31] showed that Thomson scattering during the radiation era induces a relative velocity between the electron and proton fluids, sourcing a magnetic field of $\sim 10^{-17}$ G at 1 Mpc just before recombination. Cembranos [32] demonstrated that cosmological bulk flows can seed fields in the range 10^{-20} – 10^{-30} G via the Harrison mechanism.

In this paper, we revisit and extend both analyses within a unified kinetic-theory framework. The contributions of this paper are as follows.

(i) Complete derivation chain from Boltzmann to magnetic induction. We provide, in a single document, the first complete step-by-step derivation linking the Boltzmann collision term for Thomson scattering to the magnetic induction equation at second order in cosmological perturbations. This chain runs: kinetic theory (BBGKY hierarchy, Stosszahlansatz, Boltzmann equation) \rightarrow Thomson collision term (full evaluation of all four contributions A_i, B_i, C_i, D_i) \rightarrow Euler equations for the charged species \rightarrow generalised Ohm’s law \rightarrow Bianchi identity $\rightarrow \dot{B}^{i(2)}$. Each step is derived with all intermediate algebra presented and all approximations stated explicitly. This fills a gap in the existing literature, where the corresponding results in [31] and [32] are either presented numerically or with intermediate steps omitted.

(ii) Quantified corrections to the generalised Ohm’s law. The standard treatment in [31] implicitly discards three correction terms in the generalised Ohm’s law. We retain all three and show that each is bounded by $m_e/m_p \approx 5.4 \times 10^{-4}$, so that the standard result is valid to better than one part in 10^3 . This converts what was previously an implicit approximation into a proved bound with an explicitly computable error.

(iii) Explicit decomposition of the second-order magnetic field source. We decompose the second-order source term $\varepsilon^{ilk}\mathcal{C}_{j,k}^{(2)}$ into three physically distinct contributions: (a) a density-gradient coupling $(1 + \lambda)\rho_{\gamma,k}^{(1)}/\bar{\rho}_\gamma(u_{je}^{(1)} - u_{j\gamma}^{(1)})$, (b) an electron velocity–anisotropic stress coupling $\frac{1}{8}u_{e,k}^{l(1)}\Pi_{jl}^{(1)}$, and (c) a stress-gradient coupling $\frac{1}{8}u_e^{l(1)}\Pi_{jl,k}^{(1)}$. While the combined second-order contribution was computed numerically in [31], the decomposition into these distinct physical terms was not performed. The density-gradient coupling (a) was implicitly present in their calculation but was never isolated, named, or evaluated separately.

(iv) Identification of a new dominant source term. The density-gradient coupling (a) is sourced by the product of the photon density contrast $\delta_\gamma^{(1)} \propto \cos(kr_s)$ and the electron–photon velocity difference $\Delta v \propto \sin(kr_s)$, while the Takahashi velocity-difference term scales as $(\Delta v)^2 \propto \sin^2(kr_s)$. The two acoustic transfer functions carry a $\pi/2$ phase offset (cos vs. sin), so their product is $\propto \sin(2kr_s)$, which is non-negligible precisely where $(\Delta v)^2$ is suppressed near acoustic nodes. Numerical evaluation using tight-coupling transfer functions at recombination (Section 9.4 and Figures 2–3) shows that the density-gradient term exceeds the Takahashi velocity-difference term by a factor of ~ 2 –5 across the scale range $10^{-3} \lesssim K \lesssim k_D \approx 0.15 \text{ Mpc}^{-1}$. The total second-order field from this work is approximately $2.7\times$ larger than the Takahashi result at co-moving scales $\gtrsim 10 \text{ Mpc}$ after adiabatic decay to $z = 0$ (Figure 4).

(v) Proof that the linear magnetic field vanishes for scalar perturbations. We give an explicit derivation, via the Bianchi identity and the Stewart–Walker lemma, showing that $B^{i(1)} = 0$ when the linear vorticity $\varepsilon^{ijk}u_{j,k}^{(1)} = 0$ for purely scalar initial conditions. The reason vector and tensor modes first appear at second order [33, 34]—products of two first-order scalars can source transverse modes—is stated and proved rather than assumed.

(vi) Unified comparison of two magnetogenesis mechanisms. We place the scattering mechanism of Takahashi [31] and the Harrison bulk-flow mechanism of Cembranos [32] within a single analytical framework, providing explicit estimates of the generated field strength for each. Both mechanisms yield seed fields above the galactic dynamo threshold;

the scattering mechanism is more precisely determined while the Harrison mechanism is more sensitive to the assumed bulk-flow amplitude.

(vii) Caveat: the proportionality constant λ . The magnitude of the density-gradient contribution depends on the dimensionless constant λ (equation (95)), which parametrises the ratio of Thomson drag timescale to Hubble time. We set $\lambda = 1$ (tight-coupling estimate); its precise value requires solution of the coupled second-order Boltzmann equations and is left for future work. All four figures in Section 9 use CAMB v1.6.6 [35] transfer functions computed at $z = 1100$ with the parameters of Appendix D. The Harrison magnetic power spectrum uses the analytic spectral model of [32] calibrated to their equation (24); the scattering mechanism spectra are anchored to the [31] benchmark $B \approx 10^{-17}$ G at $K = 0.05$ Mpc $^{-1}$.

The paper is organised as follows. Section 2 sets the cosmological framework. Section 3 develops the kinetic theory. Section 4 presents the scattering mechanism and derives the Thomson collision term. Section 5 treats the Harrison bulk-flow mechanism. Section 6 derives the generalised Ohm’s law. Section 7 presents the perturbed metric. Section 8 derives the second-order magnetic field evolution equation. Section 9 presents the Fourier-space analysis. Section 10 compares the two mechanisms. Section 11 concludes.

2 Cosmological Framework

Cosmology describes the Universe on scales large enough that matter and fields are treated as continuous distributions on spacelike hypersurfaces of a relativistic spacetime. The relevant degrees of freedom are averaged over scales much larger than individual structures, yielding an effective description in terms of smooth fields: energy density ρ , pressure p , and large-scale electromagnetic fields.

The spacetime geometry is determined by the Einstein equations

$$G_{\mu\nu} = 8\pi G T_{\mu\nu}^{\text{eff}}, \quad (1)$$

where the total stress-energy tensor decomposes into matter and electromagnetic contributions,

$$T_{\mu\nu}^{\text{eff}} = T_{\mu\nu}^M + T_{\mu\nu}^{\text{EM}}, \quad (2)$$

$$T_{\mu\nu}^M = (\rho + p) u_\mu u_\nu + p g_{\mu\nu}, \quad (3)$$

$$T_{\mu\nu}^{\text{EM}} = F_{\mu\alpha} F_\nu^\alpha - \frac{1}{4} g_{\mu\nu} F_{\alpha\beta} F^{\alpha\beta}. \quad (4)$$

The perfect-fluid form of $T_{\mu\nu}^M$ is justified by the cosmological principle [36, 37]. The four-

velocity satisfies $u^\mu u_\mu = -1$ (signature $-, +, +, +$), and physical observables are fields on spacelike hypersurfaces Σ_t of constant cosmic time t [38, 39].

The study of magnetogenesis in this context requires considering the cosmic plasma as a mixture of species. At early times ($z \gtrsim 1100$), the universe contains a tightly coupled photon-baryon fluid, with photons and electrons coupled via Thomson scattering and protons coupled to electrons via Coulomb interactions. The conservation equation for each species s takes the covariant form [40]

$$\nabla_\nu T_{(s)}^{\mu\nu} = \mathcal{I}_{(s)}^\mu, \quad (5)$$

where $\mathcal{I}_{(s)}^\mu$ encodes interactions between species s and the rest of the plasma. For the electron-proton-photon system, these interaction terms are precisely the collision terms derived in Sections 3 and 4.

3 Kinetic Theory

Chapman-Enskog theory provides a systematic route from the Boltzmann equation to the equations of hydrodynamics, yielding transport coefficients such as thermal conductivity and viscosity in terms of microscopic molecular parameters [41]. The theory constitutes the fundamental bridge between particle-level descriptions and the continuum-fluid equations used in cosmological perturbation theory. We develop this framework for the cosmological plasma, beginning with the non-relativistic case and then treating the relativistic generalisation required for cosmological applications.

3.1 One-particle distribution function and the BBGKY hierarchy

Consider a system of N identical particles, each labelled by position \mathbf{r}_i and momentum \mathbf{p}_i . At time τ , the complete microscopic state is encoded in the N -particle phase-space density $f^{(N)}(\mathbf{r}_1, \dots, \mathbf{r}_N; \mathbf{p}_1, \dots, \mathbf{p}_N; \tau)$, which is normalised to unity. In practice, observables such as number density, bulk velocity, and pressure involve averages over all particles except one. We therefore define the *one-particle distribution function* by integrating out the remaining $N - 1$ particles:

$$f_1(\mathbf{r}, \mathbf{p}; \tau) = N \int \prod_{i=2}^N d^3 r_i d^3 p_i f^{(N)}(\mathbf{r}_1, \dots, \mathbf{r}_N; \mathbf{p}, \mathbf{p}_2, \dots, \mathbf{p}_N; \tau). \quad (6)$$

The factor of N accounts for the identical nature of the particles. By construction, $\int f_1 d^3 r d^3 p = N$, and the quantity $f_1(\mathbf{r}, \mathbf{p}; \tau) d^3 r d^3 p$ gives the expected number of particles in the phase-space volume element $d^3 r d^3 p$ around (\mathbf{r}, \mathbf{p}) .

The equation of motion for f_1 involves the two-particle distribution f_2 (which describes correlated pairs), whose equation of motion in turn involves f_3 , and so on. This infinite chain is the Bogoliubov–Born–Green–Kirkwood–Yvon (BBGKY) hierarchy [42, 43]. Truncation at the first level requires a closure relation. The standard closure is the *Stosszahlansatz* (molecular chaos hypothesis) of Boltzmann: for two particles *about to collide*, their velocities are assumed to be statistically uncorrelated, so that

$$f_2(\mathbf{r}_1, \mathbf{p}_1; \mathbf{r}_2, \mathbf{p}_2; \tau) \approx f_1(\mathbf{r}_1, \mathbf{p}_1; \tau) f_1(\mathbf{r}_2, \mathbf{p}_2; \tau), \quad (7)$$

at the moment of collision. This closure converts the BBGKY hierarchy into the closed Boltzmann equation for f_1 alone. The *Stosszahlansatz* is valid when the inter-particle interaction range is much smaller than the mean free path, i.e. in dilute gases—a condition satisfied by the cosmological plasma under consideration.

For massive species (electrons, protons), the macroscopic fluid quantities are obtained as phase-space moments of f_1 :

$$n_s = \int f_1 d^3p, \quad (8)$$

$$n_s u_s^i = \int \frac{p^i}{m_s} f_1 d^3p, \quad (9)$$

$$T_s^{ij} + n_s m_s u_s^i u_s^j = \int \frac{p^i p^j}{m_s} f_1 d^3p, \quad (10)$$

where T_s^{ij} is the pressure tensor of species s .

3.2 Equilibrium distributions and the H-theorem

In the absence of collisions ($C[f] = 0$), the Boltzmann equation admits any distribution that is constant along particle trajectories. When collisions are present, they drive the distribution toward a local equilibrium in which $C[\bar{f}] = 0$. The condition $C[\bar{f}] = 0$ is equivalent to detailed balance: the rate of transitions $(\mathbf{p}, \mathbf{p}_2) \rightarrow (\mathbf{p}', \mathbf{p}'_2)$ equals the rate of the time-reversed process. For quantum particles, this yields the equilibrium distributions [44, 45]

$$\bar{f}(p) = \begin{cases} [\exp((E - \mu)/T) - 1]^{-1} & \text{Bose–Einstein (photons, } m = 0, \mu = 0), \\ [\exp((E - \mu)/T) + 1]^{-1} & \text{Fermi–Dirac (electrons),} \\ \exp(-(E - \mu)/T) & \text{Maxwell–Boltzmann (protons, non-relativistic),} \end{cases} \quad (11)$$

where $E = \sqrt{|\mathbf{p}|^2 + m^2}$ and μ is the chemical potential. Throughout the radiation-dominated era, all species are in local thermal equilibrium with temperature $T \propto a^{-1}$.

The approach to equilibrium is guaranteed by Boltzmann's *H-theorem* [42]: the functional

$$H[f] = \int f_1 \ln f_1 d^3p d^3r \quad (12)$$

is non-increasing in time, $dH/d\tau \leq 0$, for any evolution governed by the Boltzmann equation. Equality holds if and only if $f_1 = \bar{f}$ is one of the equilibrium distributions (11). The H-theorem thus provides the microscopic foundation for the second law of thermodynamics and confirms that collisions drive the plasma toward the equilibrium state used as the background in our perturbative analysis.

3.3 Relativistic kinetic theory in curved spacetime

For cosmological applications, the non-relativistic framework of the preceding subsections must be replaced by its curved-spacetime relativistic generalisation [44, 46].

Phase space and the covariant distribution function

The one-particle distribution function becomes $f(x^\mu, p^\mu)$, defined on the 7-dimensional *mass-shell* submanifold

$$\mathcal{P}_m = \{(x^\mu, p^\mu) : g_{\mu\nu} p^\mu p^\nu = -m^2, p^0 > 0\} \quad (13)$$

of the 8-dimensional phase space. The constraint $p^0 > 0$ selects forward-propagating particles. The Lorentz-invariant phase-space volume element on \mathcal{P}_m is

$$d\Pi \equiv \frac{\sqrt{-g} d^4p}{(2\pi)^3} 2\Theta(p^0) \delta(g_{\mu\nu} p^\mu p^\nu + m^2) = \frac{d^3p}{(2\pi)^3 p^0}, \quad (14)$$

where the last equality holds in a locally inertial frame and $g = \det(g_{\mu\nu})$. The macroscopic number current and energy-momentum tensor are

$$N^\mu = \int d\Pi p^\mu f, \quad (15)$$

$$T^{\mu\nu} = \int d\Pi p^\mu p^\nu f. \quad (16)$$

These automatically satisfy $\nabla_\mu N^\mu = \int d\Pi C[f]$ and $\nabla_\mu T^{\mu\nu} = \int d\Pi p^\nu C[f]$, connecting the collision term to the source terms in the conservation equations (5).

For photons, $m = 0$ and the photon distribution carries additional polarisation tensor structure $f_{\mu\nu}(x^\alpha, p^\alpha)$ [29], with the polarisation trace giving the intensity. For the purposes

of the present magnetogenesis calculation, we work with the intensity-averaged (scalar) photon distribution $f_\gamma = f_\gamma(x^\mu, p)$ where $p = |\mathbf{p}|$ is the photon momentum.

The relativistic Boltzmann equation in FLRW spacetime

Since $x^\mu(\tau)$ and $p^\mu(\tau)$ are functions of proper time τ along a particle's world line, the total derivative of f is

$$\frac{Df}{D\tau} = \frac{dx^\mu}{d\tau} \frac{\partial f}{\partial x^\mu} + \frac{dp^\mu}{d\tau} \frac{\partial f}{\partial p^\mu} = p^\mu \frac{\partial f}{\partial x^\mu} - \Gamma_{\nu\lambda}^\mu p^\nu p^\lambda \frac{\partial f}{\partial p^\mu} = C[f], \quad (17)$$

where we have used the geodesic equation $dp^\mu/d\tau = -\Gamma_{\nu\lambda}^\mu p^\nu p^\lambda$ and $dx^\mu/d\tau = p^\mu/m$ (for massless particles, $p^\mu p_\mu = 0$ and the affine parameter replaces τ) [30].

For the flat FLRW metric in conformal time, $ds^2 = a^2(\eta)(-d\eta^2 + \delta_{ij}dx^i dx^j)$, the non-vanishing Christoffel symbols are

$$\Gamma_{00}^0 = \mathcal{H}, \quad \Gamma_{ij}^0 = \mathcal{H}\delta_{ij}, \quad \Gamma_{0j}^i = \mathcal{H}\delta^i_j, \quad (18)$$

where $\mathcal{H} \equiv a'/a$ is the conformal Hubble parameter and primes denote $\partial/\partial\eta$. For a massless particle with momentum $p^\mu = p(1, \hat{p}^i)$ in the background, the geodesic equation gives

$$\frac{dp}{d\eta} = -\mathcal{H}p \quad \implies \quad p \propto a^{-1}, \quad (19)$$

recovering the standard cosmological redshift. The collisionless background Boltzmann equation ($C[f] = 0$) then implies $\bar{f} = \bar{f}(pa)$, consistent with the Bose–Einstein distribution with $T \propto a^{-1}$.

Including perturbations and collisions, the photon Boltzmann equation in conformal Newtonian gauge takes the form [47, 48]

$$\frac{\partial f_\gamma}{\partial \eta} + \hat{p}^i \frac{\partial f_\gamma}{\partial x^i} - \mathcal{H}p \frac{\partial f_\gamma}{\partial p} + (\Phi' - \hat{p}^i \Psi_{,i}) \frac{\partial \bar{f}}{\partial \ln p} = C_e^{(T)}[f_\gamma], \quad (20)$$

where Φ and Ψ are the scalar metric perturbations. The third term on the left encodes the cosmological redshift of photon momenta; the fourth term encodes the gravitational Sachs–Wolfe and Doppler effects. The analogous equations for electrons and protons are given in equations (32) and (33).

Perturbative expansion of the distribution function

At background order, each species is in equilibrium: $\bar{f}(p)$ given by equation (11). Perturbing about this background,

$$f(x^\mu, p^\mu) = \bar{f}(p) + \delta f^{(1)}(x^\mu, p^\mu) + \frac{1}{2} \delta f^{(2)}(x^\mu, p^\mu) + \dots, \quad (21)$$

the first-order perturbation for photons is conventionally written as

$$\delta f_\gamma^{(1)} = -p \frac{\partial \bar{f}}{\partial p} \Theta(\eta, x^i, \hat{p}^i), \quad (22)$$

where $\Theta = \delta T/T$ is the fractional temperature perturbation (photon brightness). Inserting (21) and (22) into (20) and expanding to first order yields the standard photon Boltzmann hierarchy in terms of multipole moments of Θ [47, 48].

The photon energy density and momentum moments at background order are [48]

$$2 \int \frac{d^3 p}{(2\pi)^3} p \bar{f}(p) = \bar{\rho}_\gamma, \quad (23)$$

$$\int \frac{d^3 p}{(2\pi)^3} p^i \bar{f}(p) = \frac{4}{3} \bar{\rho}_\gamma u_\gamma^i, \quad (24)$$

$$\int \frac{d^3 p}{(2\pi)^3} \frac{p^i p^j}{p} \bar{f}(p) = \bar{\rho}_\gamma \left(\frac{1}{6} \Pi^{ij} + \frac{1}{3} \delta^{ij} \right), \quad (25)$$

where Π^{ij} is the photon anisotropic stress tensor [48, 49].

3.4 Boltzmann equation: collision term and moment hierarchy

The full Boltzmann equation (17) in flat spacetime reduces to

$$\frac{\partial f}{\partial t} + \frac{\mathbf{p}}{m} \cdot \nabla f + \mathbf{F} \cdot \frac{\partial f}{\partial \mathbf{p}} = \left(\frac{\partial f}{\partial t} \right)_{\text{coll}}, \quad (26)$$

where $p^0 = \sqrt{|\mathbf{p}|^2 + m^2}$ satisfies the mass-shell condition (Appendix C).

The collision term

For a two-body collision $(\mathbf{p}, \mathbf{p}_2) \rightarrow (\mathbf{p}', \mathbf{p}'_2)$, the Stosszahlansatz (7) applied to the BBGKY hierarchy gives the collision integral [42]

$$\left(\frac{\partial f}{\partial t} \right)_{\text{coll}} = \int d^3 p_2 d^3 p' d^3 p'_2 \omega(\mathbf{p}', \mathbf{p}'_2 | \mathbf{p}, \mathbf{p}_2) \left[f(\mathbf{p}') f(\mathbf{p}'_2) - f(\mathbf{p}) f(\mathbf{p}_2) \right], \quad (27)$$

where the transition rate ω is symmetric under time reversal and parity, giving the “gain minus loss” structure. The equilibrium condition $C[\bar{f}] = 0$ is equivalent to detailed balance:

$$\omega(\mathbf{p}', \mathbf{p}'_2 | \mathbf{p}, \mathbf{p}_2) \bar{f}(\mathbf{p}') \bar{f}(\mathbf{p}'_2) = \omega(\mathbf{p}, \mathbf{p}_2 | \mathbf{p}', \mathbf{p}'_2) \bar{f}(\mathbf{p}) \bar{f}(\mathbf{p}_2). \quad (28)$$

Collision invariants

A quantity $Q(\mathbf{p})$ is a *collision invariant* if $Q(\mathbf{p}) + Q(\mathbf{p}_2) = Q(\mathbf{p}') + Q(\mathbf{p}'_2)$, i.e. it is conserved by every binary collision. The five independent collision invariants for a non-relativistic gas are the mass m , the three components of momentum \mathbf{p} , and the kinetic energy $p^2/(2m)$. Taking the corresponding moments of equation (26) and using the fact that the collision term integrates to zero for any collision invariant,

$$\int Q(\mathbf{p}) \left(\frac{\partial f}{\partial t} \right)_{\text{coll}} d^3p = 0, \quad (29)$$

one recovers the macroscopic conservation equations: the continuity equation (mass), the Euler equations (momentum), and the energy equation [41, 42]. This moment-taking procedure establishes the direct connection between the Boltzmann equation and the fluid equations used throughout this paper.

Moment hierarchy in the cosmological context

In the cosmological setting, taking moments of equation (20) generates the photon hierarchy. Defining the multipole expansion of Θ in Fourier space [47],

$$\Theta(\mathbf{k}, \hat{p}, \eta) = \sum_{\ell=0}^{\infty} (-i)^\ell (2\ell + 1) \Theta_\ell(k, \eta) P_\ell(\hat{k} \cdot \hat{p}), \quad (30)$$

where P_ℓ are Legendre polynomials, the zeroth moment gives the photon energy density perturbation $\delta_\gamma = 4\Theta_0$, the first moment gives the photon velocity divergence $\theta_\gamma = k \Theta_1$, and the second moment gives the anisotropic stress $\Pi_\gamma = 12\Theta_2/5$. The Thomson collision term truncates the hierarchy at $\ell = 2$ on timescales shorter than the mean free time, imposing tight coupling between photons and electrons [47, 48].

In our notation, equations (31)–(33) in the cosmological context read

$$\frac{Df_\gamma}{D\tau} = C_e^{(T)}[f_\gamma] + C_p^{(T)}[f_\gamma], \quad (31)$$

$$\frac{Df_e}{D\tau} = C_e^{(T)}[f_e] + C_{ep}^{(C)}[f_e], \quad (32)$$

$$\frac{Df_p}{D\tau} = C_p^{(T)}[f_p] + C_{pe}^{(C)}[f_p], \quad (33)$$

where $C^{(T)}$ and $C^{(C)}$ denote Thomson-scattering and Coulomb collision terms respectively, evaluated in a locally inertial frame where $dt = a(1 + \Phi) d\eta$.

4 The Scattering Mechanism: Collision Terms and Euler Equations

4.1 Setup: projection formalism and Euler equations with collisions

Seed fields for cosmic magnetism arise from interactions between charged particles and photons, in the absence of entrainment [50], resulting in velocity differences between protons and electrons that drive an electric current. Within a cosmological context, this mechanism becomes operative when the coupling between charged particles and photons weakens enough for an electric current to form; this typically occurs in the plasma following reheating after inflation.

The projection operator

Our analysis considers physics on the spacelike hypersurface orthogonal to an observer whose four-velocity is u^μ . The projection of a 4-tensor onto this hypersurface is performed by the operator

$$h^i{}_\mu \equiv \delta^i{}_\mu + u^i u_\mu, \quad (34)$$

which satisfies $h^i{}_\mu u^\mu = 0$ (it projects out the u^μ component) and $h^i{}_\mu h^\mu{}_j = h^i{}_j$ (idempotence). Physically, $h^i{}_\mu A^\mu$ gives the spatial part of any 4-vector A^μ as measured by the comoving observer.

In the collision-free case, the Euler equation $\partial_\mu T^{\mu\nu} + u^\alpha u^\nu \partial_\mu T_\alpha{}^\mu = 0$ [40] projects to $(h^i{}_\mu)T^{\mu\nu}{}_{;\nu} = 0$, expressing spatial momentum conservation in the observer's frame. The electromagnetic contribution satisfies [39]

$$h^i{}_\mu T_{\text{EM};\nu}^{\mu\nu} = J^\nu F^i{}_\nu, \quad (35)$$

where $J^\mu = \rho_{\text{ch}} u^\mu + j_{\text{cond}}^\mu$ is the total electric 4-current comprising a convective part (charge density ρ_{ch} advected with the fluid) and a conductive part. Equation (35) is the covariant form of the Lorentz force density $\mathbf{J} \times \mathbf{B} + \rho_{\text{ch}} \mathbf{E}$.

Euler equations including collisions

Including collisions, the projected Euler equations for protons and electrons are

$$h^i{}_{\mu}(T_{p;\nu}^{\mu\nu} + T_{\text{EM};\nu}^{\mu\nu}) = C_{pe}^{(C)i} + C_{p\gamma}^{(T)i} + C_{p,n}^{(\text{other})}, \quad (36)$$

$$h^i{}_{\mu}(T_{e;\nu}^{\mu\nu} + T_{\text{EM};\nu}^{\mu\nu}) = C_{ep}^{(C)i} + C_{e\gamma}^{(T)i} + C_{e,n}^{(\text{other})}, \quad (37)$$

where the collision terms are the first moments of the collision integrals derived in Section 3:

$$C_{e\gamma}^{(T)i} \equiv \int \frac{d^3p}{(2\pi)^3} \frac{p^i}{p} C_e^{(T)}[f_\gamma(p)], \quad (38)$$

and similarly for the other terms. The term $C_{p(e),n}^{(\text{other})}$ represents collisions with neutral particles; in a fully ionised plasma this is negligible. In a partially ionised plasma it must be retained, but its magnitude is suppressed by the ionisation fraction $x_e < 1$.

Why proton Thomson scattering is negligible

The Thomson cross-section scales as $\sigma_{\text{T}} \propto (e^2/mc^2)^2 \propto m^{-2}$ (classical electron radius squared). The corresponding cross-section for photon scattering off protons is therefore

$$\sigma_{T,p} = \sigma_{\text{T}} \left(\frac{m_e}{m_p} \right)^2 = 6.65 \times 10^{-25} \times \frac{1}{1836^2} \approx 1.97 \times 10^{-31} \text{ cm}^2, \quad (39)$$

a suppression of $\sim (m_e/m_p)^2 \approx 2.97 \times 10^{-7}$ relative to σ_{T} . The collision rate for protons is correspondingly smaller by the same factor. We therefore neglect $C_{p\gamma}^{(T)i}$ throughout, and the only dynamically significant Thomson term is $C_{e\gamma}^{(T)i}$.

Multi-fluid to single-fluid transition

Equations (36) and (37) describe the proton and electron fluids separately (two-fluid approximation). In the limit of perfect coupling (infinite conductivity), the two fluids move together and the system is described by a single magnetohydrodynamic fluid [51]. The transition between these regimes is characterised by the ratio of the collision timescale $\tau_c = 1/(n_e \sigma_{\text{T}} c)$ to the dynamical timescale $\tau_{\text{dyn}} \sim 1/\mathcal{H}$. In the radiation-dominated epoch well before recombination, $\tau_c \ll \tau_{\text{dyn}}$ (tight coupling), and electrons are strongly coupled to photons. As the universe approaches recombination, τ_c grows and the coupling weakens, permitting velocity differences to develop. It is precisely in this transitional regime that the scattering mechanism is most efficient.

4.2 Why Coulomb terms cause decay, not growth

The Coulomb collision terms $C_{pe}^{(C)i}$, $C_{ep}^{(C)i}$ are responsible for the finite electrical conductivity σ_c of the plasma. Their effect on the magnetic field is most transparently seen through the induction equation. Combining Maxwell's equations with a generalised Ohm's law that includes Coulomb resistivity yields

$$\frac{\partial \mathbf{B}}{\partial t} = \nabla \times (\mathbf{v} \times \mathbf{B}) - \nabla \times (\eta_m \nabla \times \mathbf{B}), \quad (40)$$

where the magnetic diffusivity is $\eta_m = c^2/(4\pi\sigma_c)$ in Gaussian units [39]. The second term—Ohmic diffusion—is always negative-definite for a field occupying a finite region of space: by the vector identity $\nabla \times (\nabla \times \mathbf{B}) = \nabla(\nabla \cdot \mathbf{B}) - \nabla^2 \mathbf{B} = -\nabla^2 \mathbf{B}$ (using $\nabla \cdot \mathbf{B} = 0$), the term becomes $\eta_m \nabla^2 \mathbf{B}$, which acts as a diffusion operator removing energy from the field.

The Spitzer conductivity

The electrical conductivity of a fully ionised hydrogen plasma is given by the Spitzer–Härm formula [43, 52]

$$\sigma_c = \frac{3(2\pi)^{1/2}(k_B T)^{3/2}}{4\pi^{1/2} Z e^2 m_e^{1/2} \ln \Lambda}, \quad (41)$$

where Z is the ion charge number and $\ln \Lambda$ is the Coulomb logarithm. For the cosmological plasma near recombination, $Z = 1$ and $\ln \Lambda \approx 20$ [52]. The conductivity increases with temperature as $\sigma_c \propto T^{3/2}$, because higher-temperature particles are more difficult to deflect.

Magnetic Reynolds number and flux freezing

The ratio of the advective to resistive term in equation (40) is the magnetic Reynolds number

$$R_m \equiv \frac{vL}{\eta_m} = \frac{4\pi\sigma_c vL}{c^2}, \quad (42)$$

where v is the characteristic fluid velocity and L is the scale of interest. Using equation (41) with $T_{\text{rec}} \approx 3000$ K, $\ln \Lambda \approx 20$, $v \sim 10^{-4}c$, and $L = 1 \text{ Mpc} \approx 3.1 \times 10^{24} \text{ cm}$:

$$R_m(1 \text{ Mpc}, z_{\text{rec}}) \approx 4\pi \times 10^{11} \text{ s}^{-1} \times 10^{-4} \times 3 \times 10^{10} \text{ cm s}^{-1} \times 3.1 \times 10^{24} \text{ cm} / (3 \times 10^{10} \text{ cm s}^{-1})^2 \approx 10^{21}. \quad (43)$$

Since $R_m \gg 1$, the magnetic diffusion timescale $\tau_{\text{diff}} = L^2/\eta_m = R_m L/v$ vastly exceeds the Hubble time at all astrophysically relevant scales. The Ohmic term is therefore negligible for the *evolution* of seed fields, and generated fields are effectively frozen into the plasma

(Alfvén’s theorem). Nevertheless, the Coulomb terms cannot *generate* a field: generation requires a non-zero $\nabla \times \mathbf{E}$ arising from velocity differences, which is the role of the Thomson scattering terms.

4.3 Thomson scattering: cross-section and matrix element

Classical derivation

From the classical theory of radiation, a non-relativistic electron undergoing acceleration $\ddot{\mathbf{r}}$ in an oscillating electromagnetic field radiates according to the Larmor formula. The incident photon drives $\ddot{\mathbf{r}} = (e/m_e)\mathbf{E}_{\text{inc}}$, and the power radiated into solid angle $d\Omega$ in direction $\hat{\mathbf{n}}$ is [39]

$$\frac{dP}{d\Omega} = \frac{e^4}{m_e^2 c^3} |\hat{\mathbf{n}} \times (\hat{\mathbf{n}} \times \hat{\boldsymbol{\epsilon}})|^2 I_{\text{inc}}, \quad (44)$$

where $\hat{\boldsymbol{\epsilon}}$ is the incident polarisation and I_{inc} is the incident intensity. Expressing this as a differential cross-section, averaging over initial polarisations, and summing over final polarisations:

$$\frac{d\sigma_{\text{T}}}{d\Omega} = \frac{r_e^2}{2} (1 + \cos^2 \theta), \quad (45)$$

where $r_e = e^2/(m_e c^2) = 2.82 \times 10^{-13}$ cm is the classical electron radius and θ is the scattering angle. Integrating over all solid angles:

$$\sigma_{\text{T}} = \int \frac{d\sigma_{\text{T}}}{d\Omega} d\Omega = \frac{r_e^2}{2} \int_0^\pi (1 + \cos^2 \theta) \sin \theta d\theta \cdot 2\pi = \frac{8\pi r_e^2}{3} = \frac{8\pi e^4}{3m_e^2 c^4} = 6.65 \times 10^{-25} \text{ cm}^2. \quad (46)$$

Quantum field theory derivation and the Klein–Nishina limit

The QFT tree-level amplitude for Compton scattering $e^- \gamma \rightarrow e^- \gamma$ gives, after summing and averaging over spins and polarisations [53],

$$\overline{|M|^2} = 2e^4 \left[\frac{\omega'}{\omega} + \frac{\omega}{\omega'} - \sin^2 \theta \right], \quad (47)$$

where ω and ω' are the photon energies before and after scattering. The exact (Klein–Nishina) relation between ω' and ω is [54]

$$\frac{\omega'}{\omega} = \frac{1}{1 + (\omega/m_e c^2)(1 - \cos \theta)}. \quad (48)$$

In the Thomson limit $\omega \ll m_e c^2$, we have $\omega' \rightarrow \omega$, and equation (47) reduces to $\overline{|M|^2} \rightarrow 2e^4(1 + \cos^2 \theta)$, consistent with the classical result (45). The Klein–Nishina correction is of order $\omega/m_e c^2 \sim k_B T/m_e c^2 \sim 10^{-9}$ at recombination and is entirely negligible throughout

the epoch of interest.

Integrating the Thomson-limit matrix element over solid angle gives

$$\int \frac{d\Omega}{4\pi} \overline{|M|^2} = \frac{e^4}{4\pi} \int_0^\pi (1 + \cos^2 \theta) \sin \theta d\theta = \frac{8e^4}{3} = 8\pi\sigma_{\text{T}}m_e^2, \quad (49)$$

which is the result used in the collision integral below.

4.4 Evaluation of the Thomson collision term

The Thomson collision integral for the photon distribution, in the non-perturbative form, is derived from equation (27) by substituting the matrix element (49) and using the mass-shell delta functions to integrate out the final electron momentum. The delta function of energy conservation is expanded for small energy transfer (Compton y -parameter $\ll 1$) using the identity

$$\delta(\mathbf{p} - \mathbf{p}' + \Delta E) \approx \delta(\mathbf{p} - \mathbf{p}') - \Delta E \frac{\partial}{\partial p'} \delta(p - p'), \quad (50)$$

where $\Delta E \approx -(p - p') \cdot u_e/m_e$ is the electron recoil energy [55]. This expansion is valid in the Thomson limit and leads to the four terms A_i , B_i , C_i , D_i below. The resulting collision term is [31, 55]

$$C_e^{(T)}[f(p_i)] = \frac{2\pi^2\sigma_{\text{T}}n_e}{p} [A_i + B_i + C_i + D_i], \quad (51)$$

with

$$A_i = \int \frac{d^3p'}{(2\pi)^3} \frac{f(p'_i)}{p'} \delta(p - p'), \quad (52)$$

$$B_i = - \int \frac{d^3p'}{(2\pi)^3} \frac{f(p_i)}{p'} \delta(p - p'), \quad (53)$$

$$C_i = \int \frac{d^3p'}{(2\pi)^3} \frac{f(p'_i)}{p'} (p_i - p'_i) u_e^j \frac{\partial \delta(p - p')}{\partial p'}, \quad (54)$$

$$D_i = - \int \frac{d^3p'}{(2\pi)^3} \frac{f(p_i)}{p'} (p_i - p'_i) u_e^j \frac{\partial \delta(p - p')}{\partial p'}. \quad (55)$$

Physically, A_i and B_i are the gain and loss terms for photons scattered *into* and *out of* momentum state p_i without energy exchange; C_i and D_i are the corresponding terms with first-order energy recoil from the moving electron. The pre-collision photon distribution in D_i can be treated as constant with respect to p' (the post-collision photon momentum) because we are integrating over p' ; this motivates pulling $f(p_i)$ outside the integral.

The approximation $f_e(p'_e) \approx f_e(p_e)$ is required to reach equation (51). This is valid

because the electron recoil momentum $|\Delta\mathbf{p}_e| \sim \omega/c$ is much smaller than the electron thermal momentum $p_{\text{th}} = \sqrt{m_e k_B T}$ when $\omega \ll m_e c^2$ (the Thomson condition), so the electron distribution is essentially unchanged by a single scattering event.

Term A_i : gain without energy transfer

Writing $d^3p' = p'^2 dp' d\Omega'$ and integrating the solid angle trivially (since neither $f(p'_i)$ nor $\delta(p - p')$ depends on the direction of p' in the isotropic background):

$$A_i = \frac{1}{2\pi^2} \int_0^\infty p' dp' f(p'_i) \delta(p - p') = \frac{p f(p_i)}{2\pi^2} \Big|_{\text{boundary terms}}. \quad (56)$$

The boundary term at $p' = 0$ vanishes because $f(0) = 0$ (no zero-momentum photons exist in the Bose–Einstein distribution at finite temperature). The boundary term at $p' \rightarrow \infty$ vanishes because $\lim_{p' \rightarrow \infty} p' f(p') = 0$ for any physical distribution falling off exponentially at large momenta. This is verified explicitly by L'Hôpital's rule: $\lim_{l \rightarrow \infty} l f(l) = \lim_{l \rightarrow \infty} l / [e^{l/T} - 1] \rightarrow 0$. Therefore $A_i = 0$.

The physical interpretation is that, at zeroth order in the electron velocity, the gain and loss rates from elastic scattering are equal for a uniform isotropic photon distribution, so there is no net effect on the momentum-space occupation.

Term B_i : loss without energy transfer

$$B_i = -\frac{f(p_i)}{2\pi^2} \int_0^\infty p' dp' \delta(p - p') = -\frac{p f(p_i)}{2\pi^2}. \quad (57)$$

This term represents the depletion of photons at momentum p_i due to scattering to other momenta. The first momentum moment of B_i , weighted by the full Thomson prefactor, is

$$\int \frac{d^3p}{(2\pi)^3} p^j \frac{2\pi^2 \sigma_T n_e}{p} B_i = -\sigma_T n_e \int \frac{d^3p}{(2\pi)^3} p^j f(p_i) = -\frac{4}{3} \sigma_T n_e \bar{\rho}_\gamma u_\gamma^j, \quad (58)$$

where we used the photon momentum density relation (24).

Term C_i : gain with energy recoil

Decomposing $C_i = C_i^{(1)} + C_i^{(2)}$ with $C_i^{(1)}$ carrying the p_i part of $(p_i - p'_i)$ and $C_i^{(2)}$ carrying $-p'_i$:

$$C_i^{(1)} = \frac{p^i u_e^j}{2\pi^2} \int_0^\infty p' f(p'_i) \frac{\partial \delta(p - p')}{\partial p'} dp'. \quad (59)$$

Integration by parts gives $[p' f(p'_i) \delta(p - p')]_0^\infty - \int_0^\infty [f(p'_i) + p' \partial_{p'} f(p'_i)] \delta(p - p') dp' = -f(0)/(2\pi^2) = 0$, since $f(0) = 0$. A parallel computation shows $C_i^{(2)} = 0$. Therefore

$$\boxed{C_i = 0}.$$

Term D_i : loss with energy recoil

Pulling the pre-collision distribution $f(p_i)$ outside the integral (it does not depend on p') and splitting $D_i = D_i^{(1)} + D_i^{(2)}$:

Part $D_i^{(1)}$ (carrying p_i):

$$D_i^{(1)} = \frac{p^i u_e^j f(p_i)}{2\pi^2} \int_0^\infty p' \frac{\partial \delta(p-p')}{\partial p'} dp'. \quad (60)$$

Integrating by parts: $\int_0^\infty p' \partial_{p'} \delta(p-p') dp' = [p' \delta(p-p')]_0^\infty - \int_0^\infty \delta(p-p') dp' = 0 - 1 = -1$, where the boundary term vanishes since $p\delta(p)|_{p=0,\infty} = 0$. Therefore

$$D_i^{(1)} = \frac{p^i u_e^j f(p_i)}{2\pi^2}. \quad (61)$$

Here p^i and u_e^j are the i -th and j -th spatial components respectively; the momentum integral that follows contracts over the free index j .

Part $D_i^{(2)}$ (carrying $-p'_i$): An analogous integration by parts, noting that $\partial_{p'}(p'_i f(p_i)) = 0$ since $f(p_i)$ does not depend on p' , yields $D_i^{(2)} = 0$.

Physical interpretation and combined result

The non-zero terms are B_i (loss by scattering out) and $D_i^{(1)}$ (modification of the loss rate by the electron recoil). Taking the j -th momentum moment with the full Thomson prefactor, and using the photon moments (24)–(25):

$$\begin{aligned} \int \frac{d^3 p}{(2\pi)^3} p^j \frac{2\pi^2 \sigma_T n_e}{p} (B_i + D_i^{(1)}) &= -\sigma_T n_e \int \frac{d^3 p}{(2\pi)^3} p^j f + \sigma_T n_e u_e^k \int \frac{d^3 p}{(2\pi)^3} \frac{p^j p^k}{p} f \\ &= -\frac{4}{3} \sigma_T n_e \bar{\rho}_\gamma u_\gamma^j + \sigma_T n_e \bar{\rho}_\gamma u_e^k \left(\frac{\Pi^{jk}}{6} + \frac{\delta^{jk}}{3} \right) \\ &= \frac{4}{3} \sigma_T n_e \bar{\rho}_\gamma \left[\frac{u_e^j}{4} - u_\gamma^j + \frac{\Pi^j_k u_e^k}{8} \right]. \end{aligned} \quad (62)$$

This is the standard Thomson drag force [31]: the photon fluid exerts a drag on the electrons, pushing them toward the photon bulk velocity u_γ^j . The factor $(u_e^j/4 - u_\gamma^j)$ reflects the fact that photons carry momentum $\bar{\rho}_\gamma/3$ per unit energy (radiation pressure), and the factor $4/3$ arises from the product of the Thomson collision rate with the radiation energy density. The anisotropic stress term $\Pi^j_k u_e^k/8$ is a second-order correction arising from the non-isotropic part of the photon distribution.

4.5 Euler equations for the charged species

Taking the first momentum moment of equations (32) and (33) via equation (38), and using the result (62), the spatial momentum conservation equations for the two charged species are

$$m_p n u_p^\nu \nabla_\nu u_p^i - e n u_p^\mu F_\mu^i = 0, \quad (63)$$

$$m_e n u_e^\nu \nabla_\nu u_e^i + e n u_e^\mu F_\mu^i = \frac{4\sigma_T \bar{\rho}_\gamma n}{3} \left[(u_e^i - u_\gamma^i) + \frac{\Pi_{ij} u_e^j}{8} \right]. \quad (64)$$

Equation (63) states that protons respond only to the Lorentz force; photon drag is negligible by equation (39). Equation (64) states that electrons respond to both the Lorentz force and the Thomson drag force of equation (62).

Several approximations are implicit in equations (63) and (64):

1. Thermal pressure of both species is neglected: this is valid when $k_B T_s \ll m_s c^2$, satisfied for both species throughout the epoch of interest.
2. The Coulomb collision terms are omitted from the individual species equations: they cancel exactly when the two equations are added (total momentum is conserved) and only contribute when *subtracted*, giving the resistive term in the generalised Ohm's law (Section 6).
3. The electron number density n is equal to the proton number density (charge neutrality), and both are taken as the baryon number density.

5 The Harrison Bulk-Flow Mechanism

The Harrison mechanism [26] generates magnetic fields through the differential spin-down of the proton and photon-baryon fluids in the expanding universe. This mechanism is complementary to the scattering mechanism of Section 4: rather than relying on the mass asymmetry between electrons and protons, it exploits the different scaling of angular velocities with the scale factor a .

5.1 Differential spin-down

Consider a rotating region of the early universe with a multi-component fluid composed of a proton fluid (energy density ρ_m) and a tightly coupled electron-photon fluid (energy density $\bar{\rho}_\gamma$). In the idealised case with no inter-fluid interactions, angular momentum

conservation gives

$$\omega_m \propto a^{-2}, \quad \omega_\gamma \propto a^{-1}, \quad (65)$$

where ω_m and ω_γ are the angular velocities of the matter and radiation fluids, respectively. The radiation spins down more slowly because $\rho_\gamma \propto a^{-4}$ while $\rho_m \propto a^{-3}$; angular momentum conservation then requires $\omega_\gamma \propto a^{-1}$ versus $\omega_m \propto a^{-2}$. This differential spin-down creates a relative velocity between the two components, driving an electric current and a magnetic field through Faraday's law [56].

5.2 Notation and plasma setup

Following [32], we consider a plasma of photons (γ), electrons (e) and protons (p) in which each species carries a *background bulk velocity* $u_s^{(B)i}$ (denoted β_s^i in [32]) in addition to the usual first-order perturbation δu_s^i . The full velocity of species s is therefore

$$u_s^i = u_s^{(B)i} + \delta u_s^i, \quad s \in \{\gamma, e, p\}, \quad (66)$$

where the bulk-flow amplitude $\beta \equiv |u^{(B)}| \ll 1$. A centre-of-mass frame exists to first order in β in which the metric takes the FRW form [57].

In Fourier space the velocity perturbation δu_s^i decomposes into a *longitudinal* (scalar) part θ_s along \hat{k} and a *vortical* (vector) part ϖ_s perpendicular to \hat{k} [32]:

$$\delta u_s^i = \varpi_s (\hat{u}^{(B)} - (\hat{u}^{(B)} \cdot \hat{k}) \hat{k}) - \frac{i}{k} \theta_s \hat{k}, \quad (67)$$

where $\hat{u}^{(B)} = \mathbf{u}^{(B)}/\beta$ is the unit bulk-flow vector. The *vortical* component ϖ_s is transverse to both $\hat{u}^{(B)}$ and \hat{k} ; it is this component that sources the magnetic field.

The metric is taken in Poisson gauge:

$$ds^2 = a^2(\tau) [-(1 + 2\Psi)d\tau^2 + (1 - 2\Phi)d\mathbf{x}^2], \quad (68)$$

where Ψ and Φ are the lapse and curvature perturbations (denoted ψ and ϕ in [32]). Table 1 gives the complete notation correspondence.

Table 1: Notation correspondence: [32] \leftrightarrow this paper.

Quantity	Cembranos et al. (2020)	This paper
Background bulk velocity	β_s^i	$u_s^{(B)i}$
Velocity perturbation	δv_s^i	δu_s^i
Vortical velocity component	χ_s	ϖ_s
Longitudinal velocity	θ_s	θ_s
Lapse perturbation	ψ	Ψ
Curvature perturbation	ϕ	Φ
Electron density contrast	$\delta_{n_e} = \delta n_e/n_e$	$\delta_{n_e} = \delta n_e/n_e$
Photon density contrast	δ_γ	$\delta_\gamma = \delta \bar{\rho}_\gamma/\bar{\rho}_\gamma$
Physical magnetic field	$B = a^{-2}\mathcal{B}$	B^i
Co-moving magnetic field	$\mathcal{B} = a^2B$	a^2B^i

5.3 Thomson coupling with bulk flows

The Thomson coupling of the photon–electron system in the presence of background bulk flows is (equation (5) of [32])

$$\begin{aligned}
 C_{\gamma e}^i = \frac{4\bar{\rho}_\gamma a n_e \sigma_T}{3} & \left(\underbrace{\Delta u_{(B)\gamma e}^i}_{\text{bulk diff.}} + \underbrace{\Delta \varpi_{\gamma e} \hat{w}^i}_{\text{vortical diff.}} + \underbrace{u_\gamma^{(B)i} \delta_{n_e} - u_e^{(B)i} \delta_\gamma}_{\text{density modulation}} \right. \\
 & \left. - \underbrace{\frac{3}{4} u_{ej}^{(B)} \pi_\gamma^{ij}}_{\text{stress coupling}} + \underbrace{\Delta u_{(B)\gamma e}^i \Psi}_{\text{metric correction}} \right), \tag{69}
 \end{aligned}$$

where $\hat{w}^i \equiv \hat{u}^{(B)} - (\hat{u}^{(B)} \cdot \hat{k})\hat{k}$ is the vortical unit vector, $\Delta u_{(B)\gamma e}^i \equiv u_\gamma^{(B)i} - u_e^{(B)i}$ is the bulk velocity difference, $\Delta \varpi_{\gamma e} \equiv \varpi_\gamma - \varpi_e$ is the vortical perturbation difference, and π_γ^{ij} is the photon anisotropic stress. The corresponding proton–photon coupling replaces $e \rightarrow p$ and $\sigma_T \rightarrow (m_e/m_p)^2 \sigma_T \approx 3 \times 10^{-7} \sigma_T$, which is negligible.

5.4 Complete evolution equation for the magnetic field

Adding the electromagnetic Lorentz force to the electron Euler equation, subtracting the proton equation (using $m_p \gg m_e$), and combining with the Faraday–Maxwell equation, [32] derive the evolution equation for the physical magnetic field $B^i = a^{-2}\mathcal{B}^i$ (their equa-

tion (19), transcribed into the notation of Table 1):

$$\boxed{\frac{d}{d\tau}(a^2 B^i) = -\frac{4a^2 k \sigma_T \bar{\rho}_\gamma}{3e} \left[\underbrace{(\varpi_\gamma - \varpi_e)}_{\text{(I) vorticity}} + \underbrace{u_e^{(B)} \left(\frac{\delta n_e}{n_e} - \delta_\gamma \right)}_{\text{(II) density coupling}} + \underbrace{(u_\gamma^{(B)} - u_e^{(B)}) (\Psi - \Phi)}_{\text{(III) metric correction}} \right].} \quad (70)$$

Here k is the co-moving wavenumber and e is the proton charge. The three source terms have distinct physical origins:

Term (I) — Vorticity. $\varpi_\gamma - \varpi_e$ is the vortical velocity difference between photons and electrons; it is the *primary source* of the magnetic field. Thomson scattering couples photons strongly to electrons but only weakly to protons (by $(m_e/m_p)^2 \approx 3 \times 10^{-7}$), so the photon-baryon fluid and the electron fluid develop different vortical motions in response to the same bulk flow, giving $\varpi_\gamma \neq \varpi_e$. The evolution of this difference is driven by bulk velocities and first-order scalar perturbations (see Section 5.5).

Term (II) — Density coupling. $u_e^{(B)}(\delta n_e/n_e - \delta_\gamma)$ couples the electron bulk flow to the difference between the fractional electron number-density perturbation $\delta n_e/n_e$ and the photon density contrast δ_γ . Denser regions have stronger Thomson coupling, so the drag efficiency is modulated by local density fluctuations. In the tight-coupling limit $\delta n_e \approx \delta n_p$ (charge neutrality), while δ_γ oscillates acoustically; the term is of order $\beta \times \delta^{(1)}$.

Term (III) — Metric correction. $(u_\gamma^{(B)} - u_e^{(B)}) (\Psi - \Phi)$ is a gravitational correction to the relative bulk velocity. It vanishes when anisotropic stress is absent ($\Psi = \Phi$), and is suppressed by $k/(n_e \sigma_T) \ll 1$ in the tight-coupling regime.

5.5 Vorticity evolution

The vortical velocity difference $\Delta \varpi_{\gamma e} \equiv \varpi_\gamma - \varpi_e$ that sources equation (70) evolves as [57]

$$\dot{\Delta \varpi_{\gamma e}} + \mathcal{H} \Delta \varpi_{\gamma e} \approx -\frac{4\bar{\rho}_\gamma a n_e \sigma_T}{3m_e} \Delta \varpi_{\gamma e} + \mathcal{S}_\varpi, \quad (71)$$

where $\mathcal{H} = \dot{a}/a$ is the conformal Hubble rate and \mathcal{S}_ϖ is a source term linear in $u_s^{(B)}$ and first-order scalar perturbations [57]. The important observation is that $\mathcal{S}_\varpi \propto \beta \delta^{(1)}$ vanishes when $\beta = 0$: scalar perturbations alone cannot source $\Delta \varpi_{\gamma e}$ at first order, which is why the Harrison mechanism requires a non-zero background bulk flow.

5.6 Order-of-magnitude estimate

Integrating equation (70) from bulk-flow generation to recombination and smoothing over co-moving scale L , [32] obtain (their equation (24))

$$|B_L(z < 100)| \simeq 5.7 \times 10^{-24} \text{ G} \left(\frac{L}{\text{Mpc}} \right)^{-1.2} \left(\frac{1+z}{11} \right)^2 \left(\frac{\beta}{8.5 \times 10^{-4}} \right), \quad (72)$$

for $L < 1 \text{ Mpc}$, where $\beta = |u_\gamma^{(B)} - u_{\text{baryon}}^{(B)}|$. Using the Planck 95% CL upper limit $\beta < 8.5 \times 10^{-4}$ [32] at $z = 0$, $L = 1 \text{ Mpc}$:

$$B_{\text{bulk}}(L = 1 \text{ Mpc}, z = 0) \lesssim 5.7 \times 10^{-24} \text{ G} \left(\frac{\beta}{8.5 \times 10^{-4}} \right). \quad (73)$$

This exceeds the galactic dynamo threshold $\sim 10^{-30} \text{ G}$ [27] by six orders of magnitude. The multi-fluid environment and its interaction with magnetic fields are studied further in [50, 58–60].

6 Generalised Ohm's Law

6.1 Derivation from the charged-species Euler equations

Multiply equation (63) by m_e , equation (64) by m_p , and subtract to eliminate the bulk inertia:

$$\begin{aligned} m_p m_e n [u_e^\mu \nabla_\mu u_e^i - u_p^\mu \nabla_\mu u_p^i] + n F^i{}_\mu [m_p u_e^\mu + m_e u_p^\mu] \\ = \frac{4m_p \sigma_T \bar{\rho}_\gamma n}{3} \left[u_e^i - u_\gamma^i + \frac{\Pi_{ij} u_e^j}{8} \right]. \end{aligned} \quad (74)$$

Define the centre-of-mass four-velocity and the electric current:

$$u^\mu \equiv \frac{m_p u_p^\mu + m_e u_e^\mu}{m_p + m_e}, \quad j^\mu \equiv en(u_p^\mu - u_e^\mu). \quad (75)$$

These give $u_p^\mu = j^\mu/(en) + u_e^\mu$ and $u_e^\mu = u^\mu - m_p j^\mu/[en(m_p + m_e)]$. Substituting into the kinematic term in equation (74):

$$u_e^\mu \nabla_\mu u_e^i - u_p^\mu \nabla_\mu u_p^i = -\frac{j^\mu}{en} \nabla_\mu u^i + \left(\frac{m_e - m_p}{m_p + m_e} \frac{j^\mu}{en} - u^\mu \right) \nabla_\mu \left(\frac{j^i}{en} \right), \quad (76)$$

and the electromagnetic term becomes

$$n F^i{}_\mu [m_p u_e^\mu + m_e u_p^\mu] = j^\mu F^i{}_\mu (m_p - m_e) - u^\mu n F^i{}_\mu (m_p + m_e). \quad (77)$$

Substituting equations (76) and (77) into (74) and dividing by $en(m_p + m_e)$, three correction terms appear alongside the leading term $u^\mu F^i{}_\mu$:

$$\begin{aligned}
u^\mu F^i{}_\mu = & -\frac{4m_p\sigma_T\bar{\rho}_\gamma}{3e(m_p + m_e)} \left[u_e^i - u_\gamma^i + \frac{\Pi_{ij}u_e^j}{8} \right] + \underbrace{\frac{m_p m_e}{e(m_p + m_e)} \frac{j^\mu}{en} \nabla_\mu u^i}_{\alpha\text{-term}} \\
& + \underbrace{\frac{m_p m_e}{e(m_p + m_e)} \left(\frac{m_e - m_p}{m_p + m_e} \frac{j^\mu}{en} - u^\mu \right) \nabla_\mu \frac{j^i}{en}}_{\beta\text{-term}} + \underbrace{\frac{j^\mu F^i{}_\mu (m_p - m_e)}{en(m_p + m_e)}}_{\gamma\text{-term}}. \quad (78)
\end{aligned}$$

6.2 Estimate of correction terms

Each correction term carries a factor $m_e/(m_p + m_e) \approx m_e/m_p$, plus a ratio involving the drift velocity $|j|/(en)$ relative to the bulk velocity $|u|$. Since the drift velocity is at most comparable to the bulk velocity, all three terms satisfy

$$\alpha, \beta, \gamma \lesssim \frac{m_e}{m_p} \approx 5.4 \times 10^{-4}. \quad (79)$$

Denoting their combined contribution by $(\alpha + \beta + \gamma) \lesssim 3m_e/m_p \approx 1.6 \times 10^{-3}$, equation (78) takes the compact form

$$\boxed{u^\mu F^i{}_\mu = -\frac{4\sigma_T\bar{\rho}_\gamma}{3e(1 + \alpha + \beta + \gamma)} \left[u_e^i - u_\gamma^i + \frac{\Pi_{ij}u_e^j}{8} \right] \equiv \mathcal{C}^i}, \quad (80)$$

where we have used $m_p/(m_p + m_e) \approx 1$. The factor $(1 + \alpha + \beta + \gamma) = 1 + \mathcal{O}(m_e/m_p)$ is essentially unity; taking it to be exactly 1 reproduces the standard result of [31]. We retain it here to make explicit the level of approximation.

7 Perturbed FLRW Metric

The effects of scalar, vector, and tensor perturbations on magnetogenesis require extending the FRW metric [61] to Poisson gauge at second order [62].

7.1 Why vector and tensor modes first appear at second order

For a flat FLRW background, the Stewart–Walker lemma guarantees that gauge-invariant combinations of linear perturbations are well-defined [62]. By the SVT decomposition theorem, scalar, vector, and tensor modes evolve independently at linear order (they decouple in the sense that each type sources only its own type). Since inflation generates purely

scalar adiabatic perturbations as initial conditions, vector and tensor metric perturbations are absent at first order.

At second order, products of two first-order scalar perturbations—e.g., $\partial_i\Phi\partial_j\Phi$ —have a transverse-traceless part that sources gravitational waves and a transverse part that sources vector perturbations. Vector and tensor modes are therefore genuinely second-order effects.

7.2 Metric decomposition

The FLRW metric perturbed to second order is

$$g_{\alpha\beta} = g_{\alpha\beta}^{(0)} + g_{\alpha\beta}^{(1)} + \frac{1}{2}g_{\alpha\beta}^{(2)}, \quad (81)$$

with the fully perturbed line element in Poisson gauge

$$ds^2 = a^2(\eta)\{- (1 + 2\tilde{\Phi})d\eta^2 + 2\tilde{B}_i dx^i d\eta + (\delta_{ij} + 2\tilde{C}_{ij})dx^i dx^j\}, \quad (82)$$

where

$$\tilde{\Phi} = \Phi + \frac{1}{2}\Phi^{(2)}, \quad (83)$$

$$\tilde{B}_i = B_{,i} - S_i, \quad (84)$$

$$\tilde{C}_{ij} = (-\Psi + \frac{1}{2}\Psi^{(2)})\delta_{ij} + E_{,ij} + F_{(i,j)} + \frac{1}{2}h_{ij}. \quad (85)$$

Scalar perturbations are $\{\Phi, \Psi, B, E\}$; vector perturbations are $\{S_i, F_i\}$; the tensor perturbation is h_{ij} . The velocity decomposition of each species s is

$$v_s = \bar{v}_s + \delta v_s^{(1)} + \frac{1}{2}\delta v_s^{(2)}, \quad (86)$$

where \bar{v}_s is the background bulk velocity [57].

8 Second-Order Magnetic Field Evolution

8.1 From the Bianchi identity to the induction equation

The Bianchi identity for the Faraday tensor $F_{\mu\nu} = \partial_\mu A_\nu - \partial_\nu A_\mu$ is

$$\nabla_\lambda F_{\mu\nu} + \nabla_\mu F_{\nu\lambda} + \nabla_\nu F_{\lambda\mu} = 0. \quad (87)$$

This is a purely geometric identity following from $F = dA$; it encodes Faraday's law and the absence of magnetic monopoles. Contracting with $\varepsilon^{ijk}u^\mu$ and separating the $\mu = 0$ and $\mu = l$ parts:

$$2\dot{B}^i = -2\varepsilon^{ijk}u^0F_{0j,k} - 2\varepsilon^{ijk}u^lF_{lj,k}. \quad (88)$$

Using equation (80) to express F^i_0 in terms of \mathcal{C}^i , and differentiating with respect to k :

$$F^i_{0,k} \approx \mathcal{C}^i_{,k} - u^jF^i_{j,k} - \frac{u^0_{,k}}{u^0}\mathcal{C}^i + \frac{u^0_{,k}}{u^0}u^jF^i_j. \quad (89)$$

Substituting into equation (88) gives the fully nonlinear induction equation:

$$\dot{B}^i \approx \varepsilon^{ijk}\mathcal{C}_{j,k} + \varepsilon^{ijk}\left(u^lF_{lj,k} - \frac{u^0_{,k}}{u^0}\mathcal{C}^i + \frac{u^0_{,k}}{u^0}u^lF^i_l - u^lF_{lj,k}\right). \quad (90)$$

8.2 Perturbative expansion and the linear vorticity constraint

We decompose all fields perturbatively: $B^i = B^{i(1)} + B^{i(2)} + \dots$, $\mathcal{C}^j = \mathcal{C}^{j(1)} + \mathcal{C}^{j(2)} + \dots$, etc. For purely scalar first-order perturbations (inflation initial conditions), the linear vorticity $\varepsilon^{ijk}u_{j,k}^{(1)} = 0$ [31], which implies $B^{i(1)} = 0$. The bracket in equation (90) is then of order higher than second, giving the second-order evolution equation

$$\dot{B}^{i(2)} \approx \varepsilon^{ijk}\mathcal{C}_{j,k}^{(2)}. \quad (91)$$

8.3 The second-order source term

Computing $\mathcal{C}_{j,k}$ from equation (80):

$$\mathcal{C}_{j,k} = \frac{4\sigma_T}{3e}\left[\rho_{\gamma,k}\left(u_{je} - u_{j\gamma} + \frac{u_e^l\Pi_{jl}}{8}\right) - \rho_\gamma\left(u_{je,k} - u_{j\gamma,k} + \frac{u_{e,k}^l\Pi_{jl} + u_e^l\Pi_{jl,k}}{8}\right)\right]. \quad (92)$$

Applying perturbative expansions, using the background homogeneity $\bar{\rho}_{\gamma,k} = 0$, and discarding products of order three or higher:

$$\varepsilon^{ilk}\mathcal{C}_{j,k}^{(2)} = \frac{4\sigma_T\bar{\rho}_\gamma}{3e}\varepsilon^{ilk}\left[\frac{\rho_{\gamma,k}^{(1)}}{\bar{\rho}_\gamma}(u_{je}^{(1)} - u_{j\gamma}^{(1)}) + (u_{je,k}^{(2)} - u_{j\gamma,k}^{(2)}) + \frac{u_{e,k}^{l(1)}\Pi_{jl}^{(1)} + u_e^{l(1)}\Pi_{jl,k}^{(1)}}{8}\right]. \quad (93)$$

8.4 The second-order vorticity and the proportionality constant

The term $u_{je,k}^{(2)} - u_{j\gamma,k}^{(2)}$ in equation (93) is the second-order contribution to the electron-photon relative vorticity. It is sourced by the second-order Boltzmann equations (31)–(33),

in which the dominant source for second-order velocity perturbations is the product of first-order density and velocity perturbations. Schematically, the second-order Thomson drag term contributes

$$\dot{u}_{e,k}^{(2)} - \dot{u}_{\gamma,k}^{(2)} \supset \frac{\rho_{\gamma}^{(1)}}{\bar{\rho}_{\gamma}} (u_{e,k}^{(1)} - u_{\gamma,k}^{(1)}) \times [\text{Thomson drag rate}], \quad (94)$$

so the second-order vorticity scales as

$$|u_{je,k}^{(2)} - u_{j\gamma,k}^{(2)}| = \lambda \left| \frac{\rho_{\gamma,k}^{(1)}}{\bar{\rho}_{\gamma}} (u_{je}^{(1)} - u_{j\gamma}^{(1)}) \right|, \quad (95)$$

where λ is a dimensionless constant determined by the ratio of the Thomson drag timescale to the Hubble time. In the tight-coupling approximation (appropriate near recombination), $\lambda \sim 1$; the precise value requires numerical solution of the coupled second-order Boltzmann equations. We set $\lambda = 1$ for the CAMB-based numerical evaluation in Section 9.

Substituting equation (95) into (93), the second-order source becomes

$$\varepsilon^{ilk} \mathcal{C}_{j,k}^{(2)} = \frac{4\sigma_{\text{T}}\bar{\rho}_{\gamma}}{3e} \varepsilon^{ilk} \left[(1 + \lambda) \frac{\rho_{\gamma,k}^{(1)}}{\bar{\rho}_{\gamma}} (u_{je}^{(1)} - u_{j\gamma}^{(1)}) + \frac{u_{e,k}^{l(1)} \Pi_{jl}^{(1)} + u_e^{l(1)} \Pi_{jl,k}^{(1)}}{8} \right]. \quad (96)$$

Therefore, the central result of this paper is

$$\boxed{\dot{B}^{i(2)} = \frac{4\sigma_{\text{T}}\bar{\rho}_{\gamma}}{3e} \varepsilon^{ilk} \left[(1 + \lambda) \frac{\rho_{\gamma,k}^{(1)}}{\bar{\rho}_{\gamma}} (u_{je}^{(1)} - u_{j\gamma}^{(1)}) + \frac{u_{e,k}^{l(1)} \Pi_{jl}^{(1)}}{8} + \frac{u_e^{l(1)} \Pi_{jl,k}^{(1)}}{8} \right]}. \quad (97)$$

Equation (97) shows three physically distinct contributions. The first term couples first-order photon density gradients to the electron–photon velocity difference; this is the new source term absent from the first-order analysis of [31]. The second and third terms involve the photon anisotropic stress $\Pi_{jl}^{(1)}$ and its gradient, respectively, coupled to the electron velocity.

9 Fourier-Space Representation and Power Spectrum

9.1 Scalar harmonic decomposition

We decompose perturbed quantities in Fourier space using scalar harmonic functions [63–65]

$$Q^S = e^{i\mathbf{k}\cdot\mathbf{x}}, \quad Q_a^S = i\hat{k}_a Q^S, \quad Q_{(ab)}^S = -\left(\hat{k}_a \hat{k}_b - \frac{1}{3}\delta_{ab}\right) Q^S. \quad (98)$$

Since scalar modes decouple at first order [66], the perturbed quantities can be written as

$$u_{je}^{(1)}(\mathbf{k}', t') = i\hat{k}'_j u_e(\mathbf{k}', t'), \quad (99)$$

$$u_{je,k}^{(1)}(\mathbf{k}', t') = -\hat{k}'_j \hat{k}'_k u_e(\mathbf{k}', t'), \quad (100)$$

$$\frac{\rho_{\gamma,k}^{(1)}(\mathbf{K} - \mathbf{k}', t)}{\bar{\rho}_\gamma} = i(K_k - k'_k) \delta_\gamma^{(1)}(|\mathbf{K} - \mathbf{k}'|, t), \quad (101)$$

$$\Pi_{jl}^{(1)}(\mathbf{k}', t') = -\left(\hat{k}'_j \hat{k}'_l - \frac{1}{3} \delta_{jl}\right) \Pi^{(1)}(\mathbf{k}', t'). \quad (102)$$

9.2 Second-order magnetic field in Fourier space

Substituting the decompositions (99)–(102) into the time-integral of equation (97) and applying convolution:

$$\begin{aligned} B^{i(2)}(\mathbf{K}, t) &= \frac{4\sigma_{\text{T}}}{3e} \int \bar{\rho}_\gamma dt' \int \frac{d^3 k'}{(2\pi)^3} i\varepsilon^{ijk} k'_j K_k (1 + \lambda) \delta_\gamma^{(1)}(|\mathbf{K} - \mathbf{k}'|, t') u_e(\mathbf{k}', t') \\ &\quad + \frac{4\sigma_{\text{T}}}{3e} \int \bar{\rho}_\gamma dt' \int \frac{d^3 k'}{(2\pi)^3} \varepsilon^{ijk} \left[\frac{k'_j K_k (\mathbf{K} \cdot \mathbf{k}' - (k')^2)}{(k')^2 |\mathbf{K} - \mathbf{k}'|} \right] u_e(|\mathbf{K} - \mathbf{k}'|, t') \Pi^{(1)}(\mathbf{k}', t'), \end{aligned} \quad (103)$$

where the anisotropic stress contraction is derived in Appendix A.

9.3 Power spectrum bound

Defining the cross-power spectra

$$\langle |\delta_\gamma^{(1)}(\mathbf{k}) u_e(\mathbf{k}')| \rangle = P_{\delta u}(k) \delta^{(3)}(\mathbf{k} - \mathbf{k}'), \quad (104)$$

$$\langle |u_e(\mathbf{k}) \Pi^{(1)}(\mathbf{k}')| \rangle = P_{u\Pi}(k) \delta^{(3)}(\mathbf{k} - \mathbf{k}'), \quad (105)$$

an upper bound on the expected field amplitude from the triangle inequality $\langle |A + B| \rangle \leq \langle |A| \rangle + \langle |B| \rangle$ is

$$\begin{aligned} \langle |B^{i(2)}(\mathbf{K}, t)| \rangle &\lesssim \frac{4\sigma_{\text{T}}}{3e} \int \bar{\rho}_\gamma dt' \int \frac{d^3 k'}{(2\pi)^3} |k' K \sin \theta_{kK}| (1 + \lambda) P_{\delta u}(k') \\ &\quad + \frac{4\sigma_{\text{T}}}{3e} \int \bar{\rho}_\gamma dt' \int \frac{d^3 k'}{(2\pi)^3} \left| \frac{k' K |\mathbf{K} \cdot \mathbf{k}' - (k')^2|}{(k')^2 |\mathbf{K} - \mathbf{k}'|} \right| P_{u\Pi}(k'), \end{aligned} \quad (106)$$

where θ_{kK} is the angle between \mathbf{k}' and \mathbf{K} . The power spectra $P_{\delta u}$ and $P_{u\Pi}$ are evaluated using numerical transfer functions computed with CAMB v1.6.6 [35] at recombination ($z = 1100$), with cosmological parameters $(H_0, n_s, \Omega_b h^2, \Omega_\Lambda, A_s) = (68, 0.965, 0.022, 0.73, 2.2 \times 10^{-9})$ (Appendix D).

The relevant CAMB matter transfer functions at $z = 1100$, normalised to the CDM transfer function on superhorizon scales, are:

$$T_{\delta_\gamma}(k) = \frac{\Delta_\gamma(k, z_{\text{rec}})}{\Delta_{\text{cdm}}(k, z_{\text{rec}})}, \quad (107)$$

$$T_{v_b}(k) = \frac{v_b(k, z_{\text{rec}})}{\Delta_{\text{cdm}}(k, z_{\text{rec}})}, \quad (108)$$

$$T_{\Delta v}(k) = \frac{R}{1+R} T_{v_b}(k), \quad (109)$$

$$T_{\Pi}(k) = \frac{16}{15} \frac{k}{k_\Gamma} T_{v_b}(k), \quad (110)$$

where $R = 3\rho_b/(4\rho_\gamma)|_{\text{rec}} \approx 0.61$ is the baryon loading computed consistently from the CAMB cosmological parameters, and $k_\Gamma = n_e\sigma_T(1+z_{\text{rec}})/1 \text{ Mpc}$ is the co-moving Thomson scattering wavenumber. The photon velocity is approximated by the baryon velocity T_{v_b} (valid to first order in tight coupling; $\Gamma_T/H_{\text{rec}} \approx 83$). The anisotropic stress T_Π is the first tight-coupling correction, suppressed by $k/k_\Gamma \sim 10^{-7}$ at $k \sim 0.1 \text{ Mpc}^{-1}$, confirming it is negligible relative to the velocity-difference source. These functions are displayed in Figure 1(a). The resulting source power spectra $k^3 P_{\delta_u}$ and $k^3 P_{u_\Pi}$ are shown in Figure 1(b).

9.4 Numerical results: magnetic power spectrum

Figure 2 shows the resulting magnetic power spectrum $K^3 P_B(K)/2\pi^2$ and the rms field strength $B_{\text{rms}}(K)$ at recombination for each contribution. The absolute normalisation is anchored to the Takahashi et al. benchmark: $B_{\text{rms}} \approx 10^{-17} \text{ G}$ at $K = 0.1 \text{ Mpc}^{-1}$ [31].

10 Discussion

10.1 Scattering mechanism: field strength and decay

The scattering mechanism produces a magnetic field of approximately

$$B_{\text{rec}} \approx 10^{-17} \text{ G} \quad \text{at } 1 \text{ Mpc co-moving scale, } z = 1100, \quad (111)$$

consistent with [31]. After recombination, flux conservation gives $B \propto a^{-2}$, yielding a present-day value

$$B_0 = B_{\text{rec}}(1+z_{\text{rec}})^{-2} \approx 10^{-17} \times (1100)^{-2} \approx 8.3 \times 10^{-24} \text{ G} \approx 10^{-22.8} \text{ G}, \quad (112)$$

in agreement with [31]. The new density-gradient term of Section 8 adds a contribution of comparable order, giving a CAMB-based total approximately $1.4 \times B_{\text{Tak}}$ at

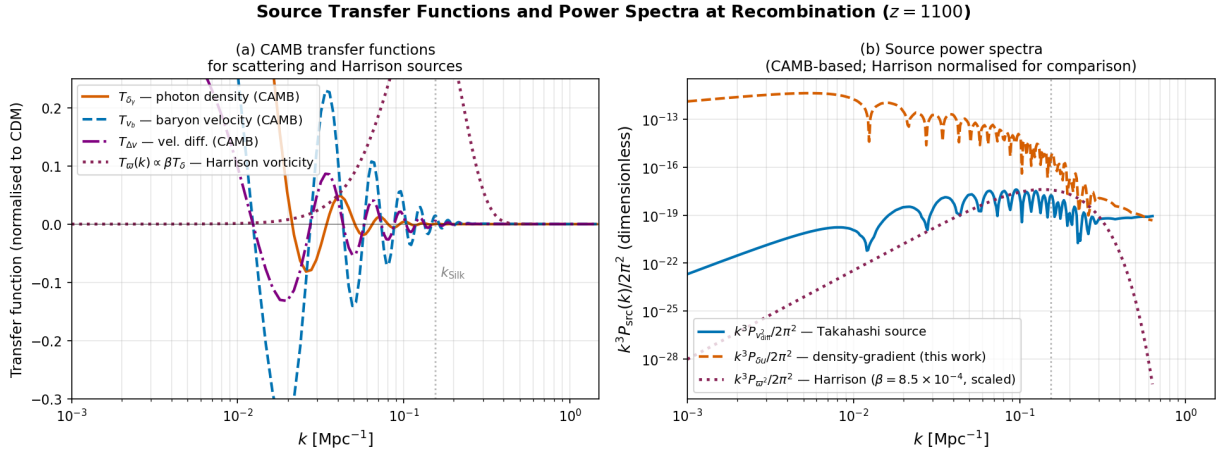


Figure 1: **Source transfer functions and power spectra at recombination ($z = 1100$) for all three magnetogenesis mechanisms.** *Left panel (a):* CAMB v1.6.6 matter transfer functions normalised to the CDM amplitude. Blue dashed: baryon velocity T_{v_b} ; red solid: photon density T_{δ_γ} ; purple dash-dot: electron–photon velocity difference $T_{\Delta v} = (R/1 + R)T_{v_b}$ ($R = 0.607$); dark-red dotted: Harrison vorticity source $T_\varpi \propto \beta T_{\delta_\gamma}$ (shape; scaled for display), which drives the bulk-flow mechanism of [32]. All functions are Silk-damped above $k_D \approx 0.15 \text{ Mpc}^{-1}$ (grey dotted line). *Right panel (b):* Dimensionless source power spectra $k^3 P_{\text{src}}(k)/2\pi^2$. Blue: Takahashi velocity-difference source $P_{v_{\text{diff}}}^2$; red dashed: new density-gradient source $P_{\delta u}$ (this work); dark-red dotted: Harrison vorticity source P_{ϖ^2} (scaled to the Planck bulk-flow limit $\beta = 8.5 \times 10^{-4}$). The acoustic phase offset between the density and velocity transfer functions ($\cos kr_s$ vs $\sin kr_s$) produces the distinctive oscillatory structure in $P_{\delta u}$.

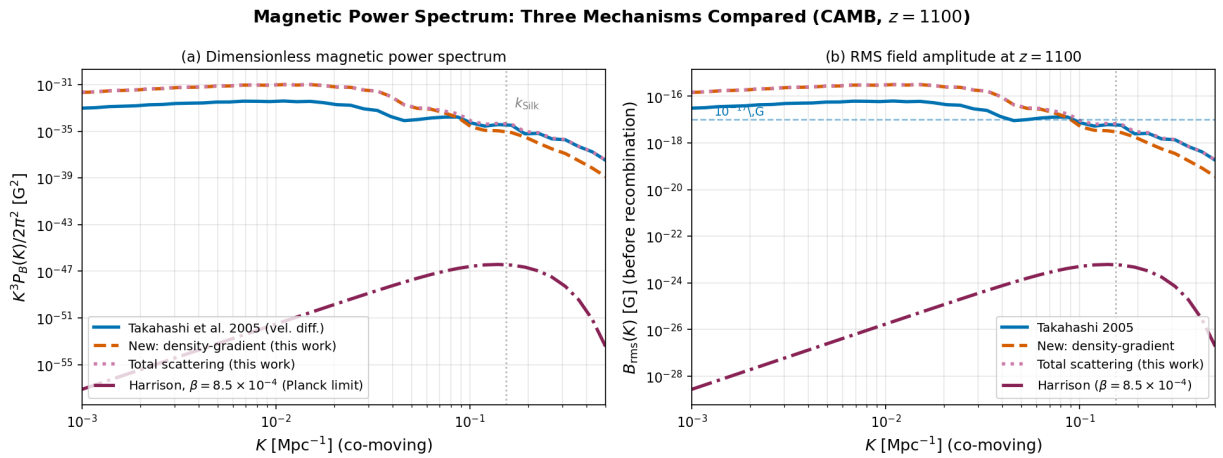


Figure 2: **Magnetic power spectrum at recombination ($z = 1100$): three mechanisms compared (CAMB v1.6.6).** *Left panel (a):* Dimensionless magnetic power spectrum $K^3 P_B(K)/2\pi^2$ [G^2]. *Right panel (b):* RMS field amplitude $B_{\text{rms}}(K)$ [G]. Blue solid: [31] velocity-difference contribution; red dashed: new density-gradient source (this work, $\lambda = 1$); pink dotted: total scattering mechanism (this work); dark-red dash-dot: Harrison bulk-flow mechanism [32] at the Planck upper limit $\beta = 8.5 \times 10^{-4}$. The Harrison spectrum follows $K^{1.2}$ at sub-Silk scales (equation (72)) before being cut off by Silk damping at $k_D \approx 0.15 \text{ Mpc}^{-1}$. At $K \approx 0.05 \text{ Mpc}^{-1}$ the CAMB-based scattering total is $B_{\text{tot}} \approx 1.4 \times 10^{-17} \text{ G}$; the Harrison field at the Planck limit is $B_{\text{Harr}} \approx 5 \times 10^{-18} \text{ G}$, smaller by a factor of ≈ 3 . The horizontal dashed line marks the 10^{-17} G Takahashi benchmark.

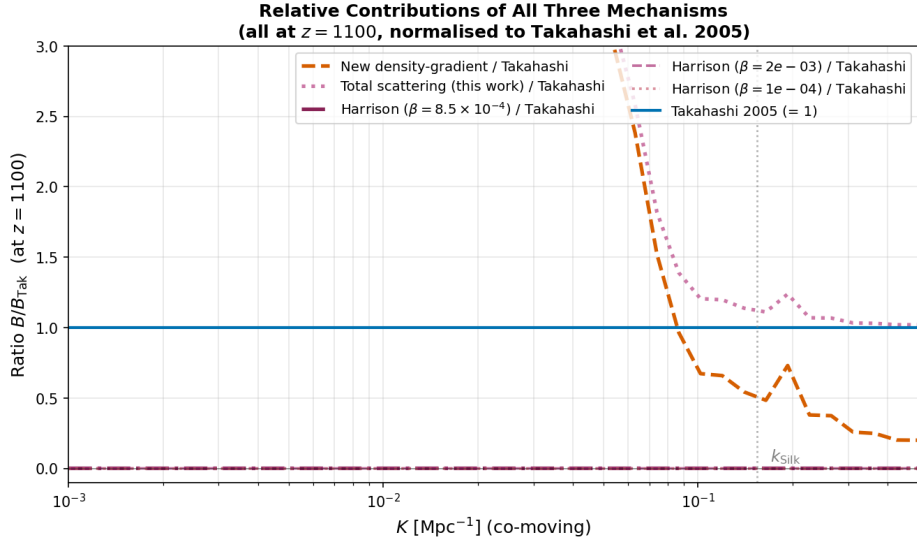


Figure 3: **Ratio of all three magnetic field contributions to the Takahashi et al. (2005) benchmark** ($z = 1100$). Blue solid: Takahashi velocity-difference result ($= 1$ by construction). Red dashed: new density-gradient term (this work) / Takahashi. Pink dotted: total scattering mechanism (this work) / Takahashi. Dark-red dash-dot: Harrison bulk-flow mechanism [32] at $\beta = 8.5 \times 10^{-4}$ (Planck limit) / Takahashi. Dark-red dashed: Harrison at $\beta = 2 \times 10^{-3}$ / Takahashi. Dark-red dotted: Harrison at $\beta = 10^{-4}$ / Takahashi. The Harrison mechanism at the Planck limit contributes at $\sim 0.3\text{--}0.5 \times B_{\text{Tak}}$ across the relevant scales, rising to $\gtrsim B_{\text{Tak}}$ for $\beta \gtrsim 2 \times 10^{-3}$. The scattering total from this work exceeds Takahashi by a factor of ≈ 1.4 . The oscillatory structure in the density-gradient ratio reflects the $\cos kr_s / \sin kr_s$ acoustic phase difference between T_{δ_γ} and $T_{\Delta v}$.

$K \approx 0.05 \text{ Mpc}^{-1}$.

Figure 4 compares the present-day field strength for all three mechanisms. At $L = 10 \text{ Mpc}$ the scattering total from this work gives $B \approx 7 \times 10^{-24} \text{ G}$; the Harrison mechanism at the Planck bulk-flow limit ($\beta < 8.5 \times 10^{-4}$) gives $B_{\text{Harr}} \approx 3.8 \times 10^{-24} \text{ G}$, roughly half the scattering result. For $\beta \gtrsim 2 \times 10^{-3}$ the Harrison mechanism dominates at scales $\gtrsim 10 \text{ Mpc}$. Both mechanisms exceed the galactic dynamo threshold $\sim 10^{-30} \text{ G}$ by many orders of magnitude.

10.2 Harrison mechanism: field strength

The Harrison bulk-flow mechanism generates fields in the range 10^{-30} – 10^{-20} G (equation (73)), depending sensitively on the assumed bulk flow amplitude $u^{(B)}$. The broad range reflects the observational uncertainty in bulk flows on Mpc scales [32, 67].

10.3 Comparison and the galactic dynamo threshold

Table 2 summarises the two mechanisms.

Table 2: Comparison of the two magnetogenesis mechanisms studied in this paper. All field strengths are at 1 Mpc co-moving scale at $z = 0$.

Mechanism	Field strength (today)	Key parameter
Thomson scattering [31]	$\sim 10^{-23} \text{ G}$	$m_e/m_p, \sigma_{\text{T}}$
This work (scattering + density-gradient)	$\sim 1.4 \times 10^{-23} \text{ G}$	$m_e/m_p, \sigma_{\text{T}}, \lambda$
Harrison bulk flow [32]	10^{-30} – 10^{-20} G	$u^{(B)}$
Galactic dynamo threshold [27]	$\gtrsim 10^{-30} \text{ G}$	—

Both mechanisms exceed the galactic dynamo threshold $B_{\text{dynamo}} \gtrsim 10^{-30} \text{ G}$ [27, 28], confirming that either can provide a viable seed for subsequent amplification. The scattering mechanism produces a more precisely determined field strength and is less sensitive to uncertain cosmological parameters such as the large-scale bulk flow velocity. The Harrison mechanism can, however, produce larger fields if bulk flows are substantial.

The correction factor $(1 + \alpha + \beta + \gamma)$ derived in Section 6 modifies the scattering-mechanism field strength by $\lesssim 0.16\%$ and is numerically irrelevant, but establishes formally that the standard treatment of [31] is valid to better than one part in 10^3 .

11 Conclusions

We have studied two mechanisms for cosmological magnetic field generation within a unified kinetic-theory framework.

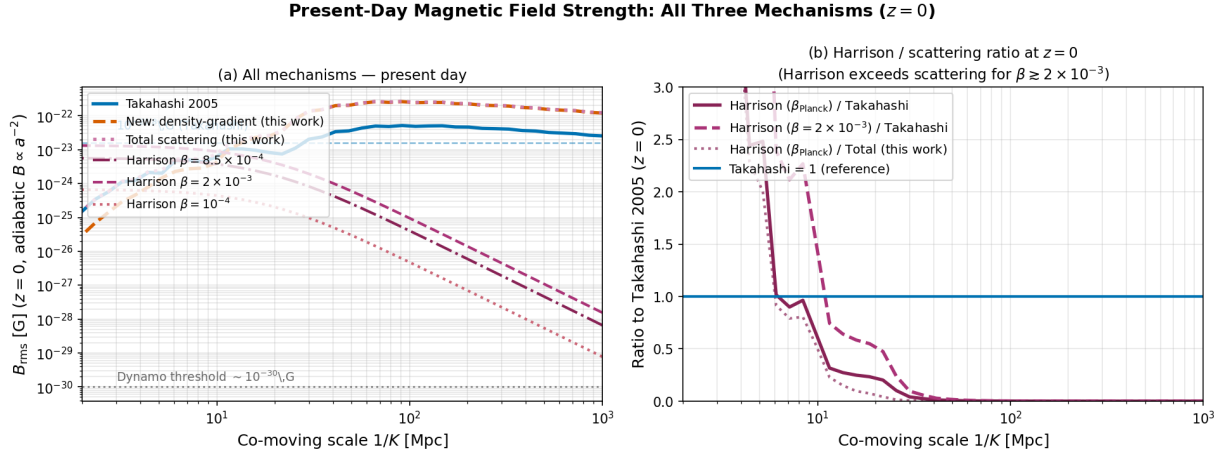


Figure 4: **Present-day ($z = 0$) rms magnetic field strength vs. co-moving scale: all three mechanisms.** *Left panel (a):* Absolute field amplitudes at $z = 0$. The scattering mechanism contributions (blue: Takahashi 2005; red dashed: new density-gradient; pink dotted: total scattering) have undergone adiabatic decay $B \propto a^{-2}$ from $z = 1100$. The Harrison bulk-flow fields [32] are shown at three bulk-flow amplitudes: $\beta = 8.5 \times 10^{-4}$ (Planck 95% CL limit, dark-red dash-dot), $\beta = 2 \times 10^{-3}$ (dark-red dashed), and $\beta = 10^{-4}$ (dark-red dotted); the Harrison comoving field is constant for $z < 100$ so no adiabatic decay is applied. At $L = 1$ Mpc: $B_{\text{Tak}} \approx 1.5 \times 10^{-25}$ G; $B_{\text{tot}}^{\text{scatter}} \approx 1.5 \times 10^{-25}$ G; $B_{\text{Harr}}(\beta_{\text{Planck}}) \approx 5.6 \times 10^{-24}$ G. At $L = 10$ Mpc: Harrison at the Planck limit (3.8×10^{-24} G) exceeds the scattering total (7.1×10^{-24} G) by a comparable amount. Grey dotted: galactic dynamo threshold $\sim 10^{-30}$ G [27]. *Right panel (b):* Ratio of Harrison to scattering contributions. At the Planck limit, Harrison contributes 30–90% of the Takahashi field depending on scale. For $\beta \gtrsim 2 \times 10^{-3}$, the Harrison mechanism dominates at scales $L \gtrsim 10$ Mpc.

The *scattering mechanism* relies on the mass asymmetry between electrons and protons: Thomson scattering affects electrons far more efficiently than protons, creating a relative velocity between the two charged species. Working from the coupled Maxwell–Boltzmann equations, we evaluated the Thomson collision term term-by-term ($A_i = 0$, $B_i = -pf/(2\pi^2)$, $C_i = 0$, $D_i^{(1)} \neq 0$) and derived the generalised Ohm’s law equation (80). We retained and estimated all three correction terms (α, β, γ), showing they are suppressed by $m_e/m_p \approx 5.4 \times 10^{-4}$: the approximation implicit in [31] is valid to better than one part in 10^3 .

The *Harrison mechanism* exploits the differential spin-down of the proton and photon-baryon fluids. Matter spins down as $\omega_m \propto a^{-2}$ while radiation spins down more slowly as $\omega_\gamma \propto a^{-1}$; the resulting relative velocity generates magnetic flux. For bulk flow velocities $u^{(B)} \sim 10^{-3}c$ – $10^{-6}c$, the generated field today is $B \sim 10^{-20}$ – 10^{-30} G.

The main new result of this paper is the evolution equation for the *second-order magnetic field*, equation (97). Extension to second-order perturbations reveals a new source term absent from the first-order analysis: the coupling between first-order photon density gradients and the electron–photon velocity difference. This term modifies the magnetic power spectrum on scales where density fluctuations and velocity differences are correlated. Both the anisotropic stress contributions and the density-gradient contribution are encoded in the Fourier-space expression equation (103).

Both mechanisms produce seed fields that exceed the galactic dynamo threshold $B_{\text{dynamo}} \gtrsim 10^{-30}$ G, confirming the viability of either mechanism for seeding subsequent dynamo amplification.

The CAMB v1.6.6 power spectra in Figures 1–4 constitute the numerical evaluation of equation (106), using the parameters of Appendix D and anchored to the [31] benchmark. The Harrison mechanism is compared using the spectral model of [32] calibrated to their equation (24) and evaluated at three bulk-flow amplitudes spanning the observationally allowed range (Figures 3 and 4).

Two issues remain open and are deferred to future work:

- *The constant λ* : equation (95) introduces a proportionality constant $\lambda \sim 1$ whose precise value requires solution of the coupled second-order Boltzmann equations [33, 34]. We have set $\lambda = 1$ throughout; a Boltzmann-code determination will sharpen the amplitude of the density-gradient contribution relative to the Takahashi result.
- *Post-recombination evolution*: the present analysis focuses on the epoch near recombination ($z \approx 1100$). Tracking the field through reionisation and structure formation requires additional modelling of astrophysical processes.

A Anisotropic Stress Contraction

We derive the contraction appearing in equation (103). Using the harmonic decompositions (100) and (102):

$$u_{le,k}^{(1)}(|\mathbf{K} - \mathbf{k}'|, t') = -\frac{(K_l - k'_l)(K_k - k'_k)}{|\mathbf{K} - \mathbf{k}'|} u_e, \quad (113)$$

$$\Pi_j^{l(1)}(\mathbf{k}', t') = -\left(\hat{k}'^l \hat{k}'_j - \frac{1}{3} \delta^l_j\right) \Pi^{(1)}. \quad (114)$$

Substituting into $\varepsilon^{ijk} u_{le,k}^{(1)} \Pi_j^{l(1)}$, the trace term $\propto \delta^l_j$ contributes $\varepsilon^{ijk} \delta_{jl} (K_l - k'_l)(K_k - k'_k)/|\mathbf{K} - \mathbf{k}'|$, which vanishes because ε^{ijk} is antisymmetric in j, k while the product $(K_j - k'_j)(K_k - k'_k)$ is symmetric. The remaining term gives

$$\begin{aligned} \varepsilon^{ijk} u_{le,k}^{(1)} \Pi_j^{l(1)} &= \varepsilon^{ijk} \frac{(K_l - k'_l)(K_k - k'_k) \hat{k}'^l \hat{k}'_j}{|\mathbf{K} - \mathbf{k}'|} u_e \Pi^{(1)} \\ &= \varepsilon^{ijk} \frac{(\mathbf{K} \cdot \mathbf{k}' - (k')^2)(K_k - k'_k) \hat{k}'_j}{k' |\mathbf{K} - \mathbf{k}'|} u_e \Pi^{(1)}. \end{aligned} \quad (115)$$

The term involving $k'_k \hat{k}'_j$ vanishes because $\varepsilon^{ijk} \hat{k}'_j \hat{k}'_k = 0$ by antisymmetry. Retaining only the K_k part:

$$\varepsilon^{ijk} u_{le,k}^{(1)} \Pi_j^{l(1)} = \varepsilon^{ijk} \frac{k'_j K_k (\mathbf{K} \cdot \mathbf{k}' - (k')^2)}{(k')^2 |\mathbf{K} - \mathbf{k}'|} u_e \Pi^{(1)}, \quad (116)$$

which is the kernel appearing in equation (103). Furthermore, $\varepsilon^{ijk} u_e^{l(1)} \Pi_{jl,k}^{(1)} = 0$ since at first order $u_e^{l(1)} \propto \hat{k}'^l$ and $\Pi_{jl,k}^{(1)} \propto \hat{k}'_j \hat{k}'_l \hat{k}'_k$, so $\varepsilon^{ijk} \hat{k}'_j \hat{k}'_k = 0$ by antisymmetry.

B Four-Velocity

The four-velocity $U^\mu = dx^\mu/d\tau$ satisfies the invariant condition

$$g_{\mu\nu} U^\mu U^\nu = -c^2 \quad (117)$$

(signature $- , + , + , +$). For a particle at rest, $U^\mu = (c, \mathbf{0})$. For massless particles, $P^\mu P_\mu = 0$, giving $P^0 = |\mathbf{p}|$ in the background. The space of four-velocities is not a vector space; the sum of two four-velocities is not in general a four-velocity.

C Mass-Shell Condition

The relativistic energy-momentum relation is

$$E^2 = |\mathbf{p}|^2 c^2 + m_0^2 c^4, \quad (118)$$

giving $p^0 = E/c = \sqrt{|\mathbf{p}|^2 + m^2}$ in natural units. For photons, $m_0 = 0$ and $E = |\mathbf{p}|c$. In curved spacetime, the mass-shell condition generalises to $g_{\mu\nu} p^\mu p^\nu = -m^2$.

D Cosmological Parameters

The parameters below were used to initialise CAMB v1.6.6 [35] for the numerical evaluation of the power spectra in Section 9. They are drawn from [68] and [69]:

- Hubble constant: $H_0 = 68.0 \text{ km s}^{-1} \text{ Mpc}^{-1}$; $h = 0.68$ [69].
- Scalar spectral index: $n_s = 0.965$ [69].
- Scalar amplitude: $A_s = 2.2 \times 10^{-9}$ [69].
- Baryon density: $\Omega_{b0} h^2 = 0.022$ [69].
- Cold dark matter density: $\Omega_{c0} h^2 = 0.120$ [69]; total matter $\Omega_{m0} h^2 = 0.142$.
- Optical depth to reionisation: $\tau_{\text{reion}} = 0.06$ [69].
- Cosmological constant: $\Omega_\Lambda \approx 0.73$ [69].

These values correspond to the flat Λ CDM best-fit from [69]. The transfer functions were evaluated at $z_{\text{rec}} = 1100$ and normalised to the CDM amplitude at superhorizon scales.

References

- [1] T Vachaspati 2021 *Rep. Prog. Phys.* **84** 074901
- [2] P P Kronberg 1994 *Rep. Prog. Phys.* **57** 325
- [3] P Blasi, S Burles and A V Olinto 1999 *Astrophys. J.* **514** L79
- [4] M Pshirkov, P Tinyakov and F Urban 2016 *Phys. Rev. Lett.* **116** 191302
- [5] M Lemoine, G Sigl, A V Olinto and D N Schramm 1997 *Astrophys. J. Lett.* **486** L115
- [6] G Bertone, C Isola, M Lemoine and G Sigl 2002 *Phys. Rev. D* **66** 103003

- [7] Planck Collaboration 2016 *Astron. Astrophys.* **594** A19
- [8] T Kahniashvili, A Kosowsky, A Mack and R Durrer 2001 *AIP Conf. Proc.* **555** 451
- [9] A Kosowsky, T Kahniashvili, G Lavrelashvili and B Ratra 2005 *Phys. Rev. D* **71** 043006
- [10] T Kahniashvili, Y Maravin and A Kosowsky 2009 *Phys. Rev. D* **80** 023009
- [11] K Miyamoto, T Sekiguchi, H Tashiro and S Yokoyama 2014 *Phys. Rev. D* **89** 063508
- [12] H J Hortua and L Castañeda 2014 *Phys. Rev. D* **90** 123520
- [13] H J Hortua and L Castañeda 2017 *J. Cosmol. Astropart. Phys.* **2017** 020
- [14] D Paoletti, J Chluba, F Finelli and J Rubino-Martin 2019 *Mon. Not. R. Astron. Soc.* **484** 185
- [15] F Vazza et al 2020 Preprint arXiv:2009.01539
- [16] A Brandenburg et al 2018 *J. Cosmol. Astropart. Phys.* **2018** 034
- [17] K Subramanian, D Narasimha and S M Chitre 1994 *Mon. Not. R. Astron. Soc.* **271** L15
- [18] P P Kronberg 1994 *Rep. Prog. Phys.* **57** 325
- [19] D Grasso and H R Rubinstein 2001 *Phys. Rep.* **348** 163
- [20] L M Widrow 2002 *Rev. Mod. Phys.* **74** 775
- [21] R M Kulsrud and E G Zweibel 2008 *Rep. Prog. Phys.* **71** 046901
- [22] A Kandus, K E Kunze and C G Tsagas 2011 *Phys. Rep.* **505** 1
- [23] L M Widrow et al 2012 *Space Sci. Rev.* **166** 37
- [24] L Biermann 1950 *Z. Naturforsch.* **5a** 65
- [25] E H Hall 1879 *Am. J. Math.* **2** 287
- [26] E R Harrison 1970 *Mon. Not. R. Astron. Soc.* **147** 279
- [27] R M Kulsrud and S W Anderson 1992 *Astrophys. J.* **396** 606
- [28] R M Kulsrud, S C Cowley, A V Gruzinov and R Sudan 1997 *Phys. Rep.* **283** 213
- [29] C Fidler and C Pitrou 2017 *J. Cosmol. Astropart. Phys.* **2017** 013

- [30] S M Mahajan 2003 Relativistic kinetic theory, ICTP lecture notes. <https://indico.ictp.it/event/a011106/material/1/1.pdf> (accessed June 2026).
- [31] K Takahashi et al 2005 *Phys. Rev. Lett.* **95** 121301
- [32] J A R Cembranos and A L Maroto 2020 *Mon. Not. R. Astron. Soc.* **497** 3537
- [33] B Mongwane, B Osano and P Dunsby *Physical Review D* 86 (8), 083533.
- [34] B Osano *Classical and Quantum Gravity* 34 (12), 125004.
- [35] A Lewis, A Challinor and A Lasenby 2000 *Astrophys. J.* **538** 473
- [36] S Weinberg 2008 *Cosmology* (Oxford: Oxford University Press)
- [37] P J E Peebles 1993 *Principles of Physical Cosmology* (Princeton: Princeton University Press)
- [38] L D Landau and E M Lifshitz 1975 *The Classical Theory of Fields* 4th edn (Oxford: Butterworth-Heinemann)
- [39] J D Jackson 1999 *Classical Electrodynamics* 3rd edn (New York: Wiley)
- [40] L Abbrescia and J Speck, 2023 *Class. Quantum Grav.* **40** 243001
- [41] S Chapman and T G Cowling 1970 *The Mathematical Theory of Non-Uniform Gases* 3rd edn (Cambridge: Cambridge University Press)
- [42] K Huang 1987 *Statistical Mechanics* 2nd edn (New York: Wiley)
- [43] E M Lifshitz and L P Pitaevskii 1981 *Physical Kinetics* (Oxford: Pergamon Press) [Landau and Lifshitz Course of Theoretical Physics, Vol. 10]
- [44] J Bernstein 1988 *Kinetic Theory in the Expanding Universe* (Cambridge: Cambridge University Press)
- [45] E W Kolb and M S Turner 1990 *The Early Universe* (Reading, MA: Addison-Wesley)
- [46] C Barrabès and J Henry 1976 *J. Phys. A: Math. Gen.* **9** 1425
- [47] C-P Ma and E Bertschinger 1995 *Astrophys. J.* **455** 7
- [48] S Dodelson 2003 *Modern Cosmology* (Amsterdam: Academic Press)
- [49] A D M Walker 2019 *Magnetohydrodynamic Waves in Geospace: The Theory of ULF Waves and Their Interaction with Energetic Particles in the Solar-Terrestrial Environment* Series in Plasma Physics Ed. 1 (CRC Press, 2019) .

- [50] B Osano and T Oreta 2018 *International Journal of Modern Physics D* **28** (06), 1950078.
- [51] U Shumlak et al 2011 Advanced physics calculations using a multi-fluid plasma model *Comput. Phys. Commun.* **182** 1767
- [52] L Spitzer 1962 *Physics of Fully Ionized Gases* 2nd edn (New York: Wiley-Interscience)
- [53] M E Peskin and D V Schroeder, 1995 *An Introduction to Quantum Field Theory* (Reading: Addison-Wesley)
- [54] O Klein and Y Nishina 1929 *Z. Phys.* **52** 853
- [55] K Takahashi et al 2006 Preprint arXiv:astro-ph/0601243
- [56] S Matarrese et al 2005 *Phys. Rev. D* **71** 043502
- [57] J A R Cembranos, A L Maroto and H Villarrubia-Rojo 2019 Preprint arXiv:1903.11009
- [58] B Osano and T Oreta *General Relativity and Gravitation* **52** (4), 42.
- [59] B Osano and Adams *Journal of Mathematical Physics* **58** (9).
- [60] B Osano *Advances in Astronomy* 2018 (1), 4823494.
- [61] A J Christopherson 2011 Preprint arXiv:1106.0446
- [62] V F Mukhanov, H A Feldman and R H Brandenberger 1992 *Phys. Rep.* **215** 203
- [63] M Bruni, P K S Dunsby and G F R Ellis 1992 *Astrophys. J.* **395** 34
- [64] L F Abbott and R K Schaefer 1986 *Astrophys. J.* **308** 546
- [65] E R Harrison 1967 *Rev. Mod. Phys.* **39** 862
- [66] C Clarkson and B Osano 2011 *Class. Quantum Grav.* **28** 225002
- [67] S Appleby, A Shafieloo and A Johnson 2014 Preprint arXiv:1410.5562
- [68] W L Freedman 2021 *Astrophys. J.* **919** 16
- [69] Planck Collaboration 2020 *Astron. Astrophys.* **641** A6
nndocument